

Strongly Interacting Two-component Coupled Bose Gas in Optical Lattices

Sagarika Basak* and Han Pu†

Department of Physics and Astronomy & Rice Center for Quantum Materials, Rice University, Houston, Texas 77251, USA

(Dated: March 11, 2022)

Two-component coupled Bose gas in a 1D optical lattice is examined. In addition to the postulated Mott insulator and superfluid phases, multiple bosonic components manifest spin degrees of freedom. Coupling of the components in the Bose gas leads to substantial change in the previously observed spin phases, giving rise to new effective spin Hamiltonian and unraveling remarkable spin correlations. The system exhibiting ferromagnetic and non-ferromagnetic spin phases for on-site intra-component interaction stronger than inter-component interaction switches from first-order to second-order phase transition between the spin phases upon introduction of coupling, on which is dependent the transition width. For comparable on-site inter- and intra- component interaction, with coupling, instead of one, two spin phases emerge with a second-order phase transition. Exact diagonalization and Variational Monte Carlo (VMC) with stochastic minimization on Entangled Plaquette State (EPS) bestow a unique and enhanced perspective into the system beyond the scope of a mean-field treatment.

Keywords: spin phase, inter-component coupling, unconventional phase, Bose–Hubbard model, Mott physics, 1D spin chains, Bose gases, adiabatic approximation

I. INTRODUCTION

Ultracold gases provide an unparalleled platform to explore physics found in atomic or molecular gases, offering a manifold of prospects to simulate and examine canonical models of strongly correlated electrons in condensed matter systems [1, 2], owing to them being clean, versatile, and highly controllable. Observation of superfluid to Mott insulator transition [3] and theoretical and experimental demonstration of exotic quantum phase transitions [4] in cold atomic setups have paved the way towards studying many-body physics [1, 2, 5–7], in association with strong correlations [3, 8], and relating to the emergence of collective and thermodynamic behavior [5, 9]. Experimental demonstrations—of cold atoms in lattices via weak trapping potential superimposed onto optical lattices [6], achievement of low temperature relevant for spin orders [1, 10–12] necessary for superexchange couplings resulting in effective nearest-neighbor spin–spin interaction demonstrated in an array of double wells [13] via a combination of evaporative and adiabatic cooling [14–21], and simulating magnetic fields via artificial gauge potential [22, 23]—provide immense relevance to this field. Quantum magnetism, a most fascinating area of research in condensed matter physics, can be reproduced using cold atoms with tunable geometry and parameters; for instance, experimental study of itinerant magnetism in ultracold Fermi systems with repulsive interactions [24], classical magnetism in triangular lattices [25] with fast oscillations of optical lattice enabling tuning the sign of nearest-neighbor tunneling [26], bosons with strong interactions in a tilted lattice at commensurate fillings for study of Ising model and quantum phase transition [27, 28] and possible realization of quantum dimer

models [27, 29].

Bose–Hubbard Hamiltonian describing the dynamics of bosonic atoms is a quintessential model to probe strongly correlated many-body quantum systems [5, 30, 31] and simulate lattice spin models [1, 2, 31–39] such as quadratic-biquadratic spin model [40], or antiferromagnetic spin chains [27] and spin-1 model exhibiting Haldane (gapped) insulator phase [41–45]. Interesting extensions of Bose–Hubbard model, such as inclusion of next-to-nearest-neighbor tunneling or long range interactions [46–51], spinor bosons with multiple internal degrees of freedom [52, 53] and addition of nonlinear coupling between the components [54–59], display remarkably rich phase diagrams [47, 56–59]. A two-component Bose–Hubbard in Mott phase reveals pseudospins effectively coupled by Heisenberg exchange [38] imitating spin- $1/2$ Hamiltonian ideal for study of quantum magnetism [38, 60, 61], displays a spin-Mott phase in spin-1 Hamiltonian [11, 38, 39, 60, 62, 63], and in the presence of strong repulsions presents finite-temperature phase structure with possibility of checkerboard long range order, supercounterflow, superfluidity, and phase separation [64]. Realization of controllable Bose–Bose mixtures [65] makes way for the experimental reproduction of spin Hamiltonians, with detection and study of magnetic phases such as antiferromagnetic Néel and xy ferromagnetic phases.

The physics of coherent coupling in ultracold gases is consequential for quantum information processing and simulation [31, 37]; supported by the demonstration of strong coupling between Bosonic Mott insulators and light [66, 67] and the recent work in cold atoms proposing the realization and manipulation of new quantum states [68–75] and high precision quantum limited measurements [76]. In the two-component Bose gas, introducing coupling reveals fascinating physics; for instance, the phase separation in weak interaction limit [77] changing dramatically [78–89], modifying the Mott-insulator–superfluid transition [90], and altering entanglement properties [91]. With the introduction of nonlinear coupling in many-body systems, stable collective modes appear, thus paving the way for robust control [92, 93], with their localization properties and robustness against perturba-

* basak.sagarika@rice.edu

† hpu@rice.edu

tions demonstrated in a tilted Bose–Hubbard model [94].

Here, we study Bose gas with two components trapped in a one-dimensional (1D) optical lattice, realizing a two-component Bose–Hubbard Model. Presence of multiple bosonic components manifests spin degrees of freedom in addition to Mott insulator and superfluid phases [38, 60]. The coupling of the two components on the nearest-neighboring sites with strong on-site interactions presents unconventional effective ordering generating unprecedented spin behavior. The formation of a new site-dependent non-ferromagnetic spin phase occurs owing to this coupling. The choice of spin alignment along z in this phase can be tuned using hopping parameters. The signature of this unique phase appears as oscillation in spatial z - x spin correlation between spins, whereas remaining constant (~ 0) in a conventional anti-ferromagnetic spin phase. In addition to the creation of the unconventional non-ferromagnetic spin phase, the coupling also significantly alters the phase space. When the intra-component interaction is stronger than the inter-component interaction, the introduced coupling switches the phase transition between ferromagnetic and non-ferromagnetic spin phases from first-order to second-order, with the transition width dependent on coupling. When these interactions are comparable, two spin phases (ferromagnetic and non-ferromagnetic) are displayed instead of one (ferromagnetic) with a second-order phase transition, when coupling is introduced. This study provides a spin-independent implementation of the optical lattice for trapping the two-component Bose gas with no additional tuning of on-site interaction strengths and instead leveraging coupling as a parameter to switch between the different spin phases. Multiple perspectives—obtained from methods based on mean-field approximation, exact diagonalization, and entangled-plaquette states (EPS)—enhance the understanding of this system; capturing correlations beyond the scope of a mean-field treatment. The physics of filling factor greater than unity where the novel spin correlations persist, and the consideration of complex intra-component tunneling and inter-component coupling are discussed.

This paper is sectioned as follows: Sec. II describes the coupled two-component Bose–Hubbard model and its realization. Sec. III details the mapped spin- $1/2$ model. Sec. IV presents the different numerical methods considered in the study. Sec. V is the multi-perspective study of the spin phases. Sec. VI extends to discuss complex intra-component tunneling and inter-component coupling as well as the physics of occupancy greater than unity. Finally, Sec. VII summarizes the results and discusses their implications and future avenues.

II. THE MODEL

We consider a 1D system comprising two kinds of bosons trapped in a spin-independent optical lattice as shown in Fig. 1. The two components termed as a and b , can be envisioned as two internal levels of an atom. We assume low temperature and the optical lattice to be deep enough for the atoms to be confined to the lowest Bloch band describing a two-component Bose–Hubbard model [39, 95]. The optical

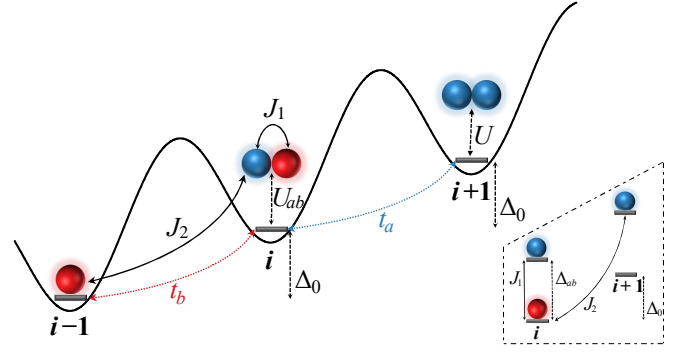


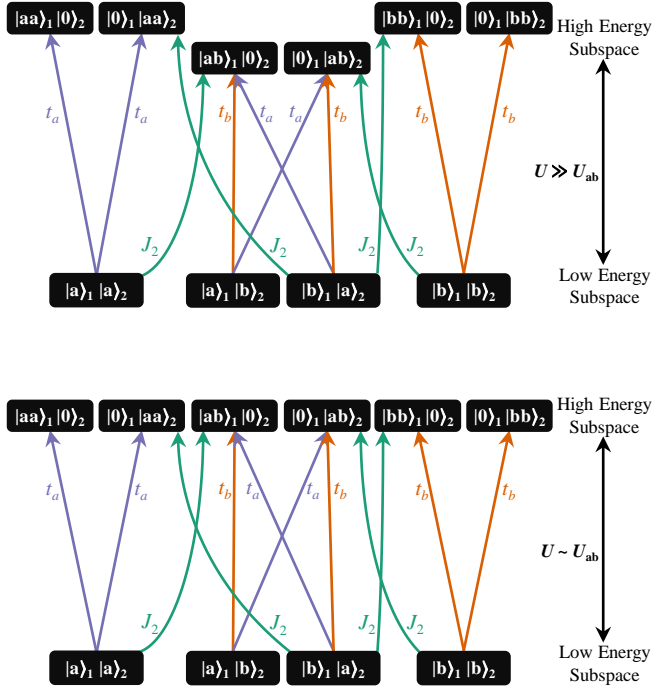
FIG. 1. (color online) Two-component Bose–Hubbard model with on-site inter- (U_{ab}) and intra- (U) component interaction ($U \gg U_{ab}$ and $U \sim U_{ab}$) with nearest-neighbor tunneling coefficients t_a and t_b . The optical lattice is tilted via external inhomogeneous static electric or magnetic field. *Inset*: To the system is introduced laser-assisted inter-component coupling: J_1 (same-site) and J_2 (nearest-neighbor). The two components are visualized as two levels of an atom.

lattice is tilted, creating an energy offset between the neighboring sites as shown in Fig. 1, with the assumption that the potential applied to create this tilt is a perturbation. This tilt can be introduced using a magnetic field gradient [96, 97]. The tilting of the lattice prevents the natural hopping between components a (or b) which is obtained via light assisted tunneling: resonant two-photon Raman transition [96]. We introduce to this system inter-component coupling; also obtained by a resonant two-photon Raman transition between two internal states as shown in Fig. 1 (*inset*). The resulting system is governed by the following Hamiltonian:

$$\begin{aligned}
 H = & \sum_i (-t_a a_i^\dagger a_{i+1} - t_b b_i^\dagger b_{i+1} + H.c.) \\
 & + \sum_{k=a,b;i} \frac{U}{2} n_{ki}(n_{ki}-1) + \sum_i U_{ab} n_{ai} n_{bi} \\
 & - \sum_i J_1 (a_i^\dagger b_i + b_i^\dagger a_i) - \sum_i J_2 (b_i^\dagger a_{i+1} + a_{i+1}^\dagger b_i),
 \end{aligned} \tag{1}$$

where a_i and b_i are the bosonic annihilation operators for components a and b at site i , respectively. t_k is the component-dependent tunneling parameter, U and U_{ab} are the intra- and inter-component on-site interaction strengths, respectively. Two kinds of inter-component couplings are present: J_1 and J_2 representing the same-site and nearest-neighbor coupling, respectively. The energy offset between nearest-neighboring sites of the optical lattice (Fig. 1) differentiates the couplings, where J_2 defines the inter-component coupling between b at site i and a at site $i+1$. The presence of this offset also allows for tuning of J_1 and J_2 independently (Fig. 1 *inset*). In the deep Mott limit ($U, U_{ab} \gg t_k, J_1, J_2$), with the average number of particles per site being fixed due to the high energy cost of bosons hopping from one site to another, this model can be mapped to an effective spin system. In the following sections we study the system in the deep Mott limit, specifically for the case of one particle per site that is mapped to spin- $1/2$, where a : \uparrow and b : \downarrow .

(a)



(b)

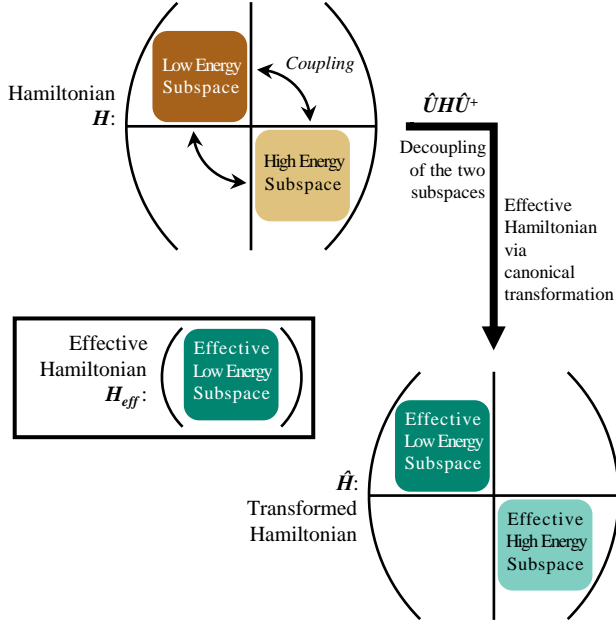


FIG. 2. (color online) Schematic of the effective spin Hamiltonian. (a) The low- and high-energy subspaces for a two-site system, roughly separated by the on-site interaction strength and coupled by the inter-component coupling and intra-component tunneling coefficients. (b) The Hamiltonian with low and high-energy subspaces forming the diagonal with the off-diagonal coupling and tunneling coefficients coupling the two subspaces and the effective decoupling of the two subspaces to obtain the effective low-energy spin Hamiltonian.

III. EFFECTIVE SPIN HAMILTONIAN

Strong on-site interactions divide the Hilbert space into low-energy and high-energy subspaces, which are coupled by the coupling and tunneling terms as shown in Fig. 2. A particle hopping from one site to another increases the occupancy, thus going from a low-energy to high-energy subspace, and thus incurring high energy cost in the process. Whereas, two particles exchanging positions preserve the occupancy and hence do not require a high energy cost. To study the relevant physics, the effective low-energy subspace is obtained by decoupling the existing subspaces; removing any first-order hopping that increases the occupancy and retaining the second-order virtual hopping terms that preserve the occupancy.

The two-component Bose–Hubbard model mapped to the following effective spin (low-energy) Hamiltonian via canonical transformation and followed by a perturbative expansion up to second-order (for details, see Appendix A):

$$H_{\text{eff}} = \sum_i \left[-J_{\perp} (\sigma_i^x \sigma_{i+1}^x + \sigma_i^y \sigma_{i+1}^y) - J_z \sigma_i^z \sigma_{i+1}^z - h_z (\sigma_i^z) - (h_x + J_1) \sigma_i^x + J_{zx} \sigma_i^z \sigma_{i+1}^x - J_{xz} \sigma_i^x \sigma_{i+1}^z \right], \quad (2)$$

where $J_{\perp} = t_a t_b / U_{ab}$ and $J_z = (t_a^2 + t_b^2 - J_2^2) / U + (t_a^2 + t_b^2 - J_2^2) / 2 U_{ab}$ provide the xy and z ordering respectively. The xy ordering is always ferromagnetic in nature, while the z ordering can be tuned from ferromagnetic to anti-ferromagnetic by varying the parameters t_a , t_b , and J_2 . The terms $h_z = 2t_a^2/U - 2t_b^2/U$ and $h_x = J_2(t_a + t_b)(1/U_{ab} + 1/U)$, J_1 act as fictitious magnetic fields along z and x , respectively, transforming the system to a spin-polarized state. Unconventional ordering terms, $J_{zx} = J_2 t_b / U$ and $J_{xz} = J_2 t_a / U$ arise due to the directional nearest-neighbor inter-component coupling. They tend to align the spins along x on one site and along z on the neighboring sites providing a straightforward implementation for site-dependent spin alignment. Presently only J_2 is considered as J_1 , with no energy cost in same-site coupling, trivially leads the system to an x ferromagnetic phase. With the introduction of nearest neighbor inter-component coupling, we see new ordering terms h_x , J_{zx} , and J_{xz} ; their significance is understood by studying the system behavior dictated by parameters t_a , t_b , and J_2 .

IV. NUMERICAL METHODS

Three different methods are utilized in our study: (a) mean-field approximation, (b) exact diagonalization for small system size ($N < 14$), and (c) Variational Monte Carlo with stochastic minimization (VMC-SM) on Entangled-Plaquette States (EPS) for large system size ($N \geq 14$).

Mean-field approximation is the simplest approach pursued. Here, each site is treated independent of the others, making it computationally efficient. Additionally, it is unaffected by the system size. To illustrate the spin phases within mean-field, we designate each alternating site to subspace A and its neighboring sites to B . The following variational ansatz

is considered:

$$|\Psi\rangle = \prod_{i \in A} (\cos(\theta_A)|a\rangle_i + \sin(\theta_A)|b\rangle_i) \prod_{i+1 \in B} (\cos(\theta_B)|a\rangle_{i+1} + \sin(\theta_B)|b\rangle_{i+1}) \quad (3)$$

Within mean-field approximation, the spin order along x and z computed using Pauli matrices:

$$\langle \sigma_{i \vee i+1}^x \rangle = \sin 2\theta_{A \vee B}, \quad \langle \sigma_{i \vee i+1}^z \rangle = \cos 2\theta_{A \vee B} \quad (4)$$

The simplicity of mean-field approximation, in treating each site independent of others, may not accurately reflect the system behavior due to the presence of spin exchanges in the effective spin Hamiltonian correlating neighboring sites. This could dilute the effect of the unconventional correlations by their being beyond the scope of the mean-field treatment.

Exact diagonalization provides the most accurate description of the system. Devoid of any approximations, it is the most successful in capturing the effect of the unconventional correlations. Additionally it provides direct comparisons to $N = 2$ (see Appendix B), where the effective spin Hamiltonian (2) is benchmarked against the original Hamiltonian (1) and validated. Although the exact diagonalization does provide a better insight into the system, owing to its large computational expense, this is limited to smaller system sizes $N < 14$, where the effect of small system size can be observed. For the thermodynamic limit, this demands a numerical method that captures correlations better than mean-field but with lesser computation cost than exact diagonalization.

Entangled-Plaquette States (EPS) form a class of tensor network states, where the lattice is divided into plaquettes, and the wave function of the system is given by the product of the plaquette wave functions which are scalar in nature [98]. This goes beyond the mean-field, by considering overlapping or entangled-plaquettes, and is more computationally efficient than exact diagonalization as the number of steps to obtain the system ground state undergo a low order polynomial increase with system size. It allows for large system sizes while retaining most of the effects of the correlations. The state for the system is a sum over all possible spin configurations (\mathbf{n}) with each configuration weighted by amplitude $W(\mathbf{n})$ [99]:

$$|\Psi\rangle = \sum_{\mathbf{n}} W(\mathbf{n})|\mathbf{n}\rangle; \quad \mathbf{n} = n_1, n_2, n_3, \dots, n_N,$$

where $n_i = \pm 1$. In our ansatz with overlapping plaquettes (P), each consisting of four sites, coefficients ($C_P^{\mathbf{n}P}$; correlator elements) are assigned for all 2^4 possible configurations in each plaquette. The amplitude ($W(\mathbf{n})$) for each spin configuration in the state is given as a product of these correlator elements [99]:

$$W(\mathbf{n}) = \prod_{P=1}^{N/2} C_P^{\mathbf{n}P} = C_1^{n_1, n_2, n_3, n_4} C_2^{n_3, n_4, n_5, n_6} \dots C_{N/2}^{n_{N-1}, n_N, n_1, n_2}$$

Variational Monte Carlo (VMC) with stochastic minimization (SM) is used to obtain the optimized plaquette wave functions that minimize the energy and best describe the ground state [98].

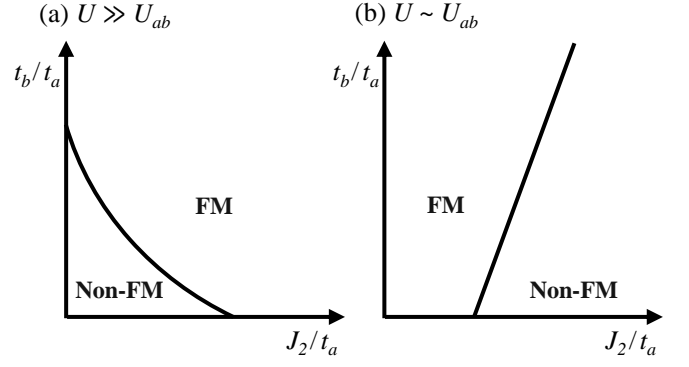


FIG. 3. Schematic of spin phases hypothesized to emerge in the presence of inter-component coupling (J_2). The phases are shown in the deep Mott regime, (a) $U \gg U_{ab}$ and (b) $U \sim U_{ab}$, and presented as a function of scaled intra-component tunneling t_b/t_a and inter-component coupling J_2/t_a .

Concurrent employment of all three methods in our analysis helps in validating each method and identifying areas where they fail. It also facilitates an accurate interpretation of the results that best reflect the system behavior, with minimal effect of system size and mean-field biases.

V. SPIN PHASES

Previous work studying the two-component Bose–Hubbard model in the absence of inter-component coupling, shows two spin phases xy ferromagnetic (FM; $t_a \sim t_b$), and z anti-ferromagnetic (AFM; $t_{a \vee b} \gg t_{b \vee a}$) with a first-order phase transition [39]. This is only seen in the on-site interaction limit $U \gg U_{ab}$. In the other on-site interaction limit $U \sim U_{ab}$, no phase transition occurs with only one spin phase: z FM. Motivated by these, we explore the spin phase space in the presence of coupling at strong on-site intra- and inter-component interaction: $U \gg U_{ab}$ and $U \sim U_{ab}$. A schematic of the spin phases in the presence of coupling is surmised from the effective Hamiltonian as shown in Fig. 3. Introducing J_2 , the system with $t_{a \vee b} \gg t_{b \vee a}$ demonstrating a z AFM in the non-FM phase, evolves to a unconventional non-FM phase arising due to J_{xz} and J_{zx} . The orientation of the spin in this phase depends on t_a and t_b . With further increase in J_2 , this transitions to x FM in the FM phase due to h_x , eventually evolving to a z FM phase at $U \gg U_{ab}$ due to J_z . A system around $t_a \sim t_b$ displays xy FM phase in the absence of coupling and becomes an x FM due to h_x in the presence of coupling. In the limit $U \sim U_{ab}$, with increasing J_2 , the system evolves from a biased z FM to x FM in the FM phase, transitioning to the unconventional non-FM and evolving to a z AFM in the non-FM phase.

In this section, we study the spin phases that arise in the system under consideration here by evaluating the spin order parameters. The presence of the site-dependent nature of the unconventional phase emerging due to the unique correlations are confirmed with the examination of the correlation between spins at two different sites. The spin orders along z and x on

neighboring sites depict the existence of two phases in our system, spins aligning along the same direction (FM) at large tunneling (t_b/t_a) or coupling (J_2/t_a) for $U \gg U_{ab}$ or at tunneling (t_b/t_a) comparable or stronger than coupling (J_2/t_a) for $U \sim U_{ab}$ and spins aligning along different directions (Non-FM) otherwise, as seen in Figs. 4 and 5. Figs. 4 & 5 (a i & a ii) representing the spin behavior along z in the mean-field limit, displays one of the degenerate spin configuration on the neighboring sites in the Non-FM phase, whereas Figs. 4 & 5 (b i & b ii) obtained via exact diagonalization with periodic boundary conditions shows a superposition of the degenerate spin configuration. In both $U \gg U_{ab}$ and $U \sim U_{ab}$ limits, the system in the presence of coupling shows a second-order phase transition. The phase transition between the two phases appears as a discontinuity in the spin orders as seen in Figs. 4 and 5. The critical expression for tunneling t_b/t_a as a function of coupling J_2/t_a , and interactions U, U_{ab} describing the phase boundary can be found analytically within the mean field treatment (see Appendix C):

$$(t_b/t_a)_{U \gg U_{ab}}^C = - \left(\frac{J_2/t_a(U + U_{ab}) + 2U}{2(2U_{ab} - U)} \right) - \sqrt{\left(\frac{J_2/t_a(U + U_{ab}) + 2U}{2(2U_{ab} - U)} \right)^2 - \left(1 - J_2^2/t_a^2 + \frac{J_2/t_a(U + U_{ab})}{2U_{ab} - U} \right)} \quad (5)$$

$$(t_b/t_a)_{U \sim U_{ab}}^C = - \left(\frac{J_2/t_a(U + U_{ab}) + 2U}{2(2U_{ab} - U)} \right) + \sqrt{\left(\frac{J_2/t_a(U + U_{ab}) + 2U}{2(2U_{ab} - U)} \right)^2 - \left(1 - J_2^2/t_a^2 + \frac{J_2/t_a(U + U_{ab})}{2U_{ab} - U} \right)} \quad (6)$$

The spin correlation ($\langle \sigma_i \cdot \sigma_{i+1} \rangle$) between the neighboring sites is presented in Fig. 6, which demonstrates the Non-FM (< 1) phase and the FM ($= 1$) phase, with the approximate critical tunneling coefficient t_b/t_a describing the phase boundary. At $U \gg U_{ab}$, a first-order transition occurs along the vertical axis (i.e., $J_2 = 0$), which shifts to a second-order transition as the coupling is introduced, with the transition width increasing with coupling. The spin correlation obtained via exact diagonalization confirms the existence of the two spin phases. The difference between the mean field approximation and exact diagonalization is expected on account of the smaller system size in ED and the treatment of all sites independent of each other in mean field.

$U \gg U_{ab}$: In the absence of coupling, dependent on the two competing energy parameters J_z and J_\perp in the Hamiltonian, the system displays zAFM for $J_z \geq J_\perp$ and xyFM for $J_z < J_\perp$ spin phases [39]. These phases appear due to the high energy cost of the intermediate state $|aa\rangle_j$ or $|bb\rangle_j$ when compared to $|ab\rangle_j$, resulting in high tunneling probability for states $|a\rangle_j|b\rangle_{j+1}$ or $|b\rangle_j|a\rangle_{j+1}$.

Introducing coupling to this system, evolves the conventional zAFM spin phase to a remarkable site and intra-component tunneling dependent spin phase termed as the unconventional Non-FM phase as depicted in Fig. 4. The coupling in the system, allows component b on some site j to

tunnel to a on site $j+1$ or vice versa, thus allowing the neighboring sites to have the same component, where the hopping of the components results in $|ab\rangle_j$ intermediate state. The phase demonstrates a stronger z order at one site and x order at the neighboring sites in the mean-field limit. Spin orientation along z depends on the intra-component tunneling, with up spin at $t_b/t_a < 1$ and down spin at $t_b/t_a > 1$. The observed unconventional phase emerges due to correlations induced by the J_{xz} and J_{zx} terms, and is preferentially chosen by the effective ordering h_x and h_z .

The system transitions to the FM phase forming an xFM phase upon further increase of the coupling or tunneling. At large tunneling and in the absence of coupling, an xyFM phase is resulted as shown in the previous work [39]. However, this preference changes with the introduction of coupling as seen in Fig. 4, forming an xFM phase, owing to the strong h_x ordering.

$U \sim U_{ab}$: In this limit, all the high-energy intermediate states have equivalent energy cost associated with them unlike the previous interaction limit. In a strong coupling limit ($J_2/t_a \gg t_b/t_a, 1$), the conventional zAFM spin phase emerges due to the strong effective ordering along z : J_z as seen in Figs. 5(a i) and 5(a ii). With no significant intra-particle tunneling, only the component b at some site j is allowed to tunnel to a at site $j+1$, and vice versa, resulting in highest delocalization of configuration $|a\rangle_j|b\rangle_{j+1}$ or $|b\rangle_j|a\rangle_{j+1}$, allowing the formation of the observed zAFM phase.

Allowing one component to tunnel by a small increase in intra-component tunneling $t_{a\vee b}$ ($J_2 > t_{a\vee b} > t_{b\vee a}$), the site and intra-component tunneling dependent spin phase materializes forming the unconventional non-FM phase as depicted in Fig. 5. When one component's intra-component tunneling is as strong as the coupling ($J_2 \sim t_{a\vee b} \gg t_{b\vee a}$), the FM phase exists. When a component is allowed to tunnel, preference of that component on all sites is expected; this leads to the spin up zFM for $t_a \gg t_b$ and spin down zFM for $t_b \gg t_a$ as seen in Figs. 5(ai), 5(a ii), 5(b i) and 5(b ii). However, this preference changes with strong coupling as seen in Fig. 5, with simultaneous non-vanishing of σ_z and σ_x , which exist on nearest-neighboring sites owing to the strong J_z , h_z , and h_x ordering eventually forming an xFM phase at stronger coupling, due to h_x ordering. With both components being allowed to hop, all sites have equal presence of components a and b . The spin correlations obtained via exact diagonalization are comparable to the mean-field treatment for correlations along z and x .

Unconventional Non-FM: The spin orders in exact diagonalization do not display the conventional zAFM and the unconventional non-FM phase as seen in the mean field. The mean field shows one of the degenerate configurations as a result of spontaneous symmetry breaking, whereas the exact diagonalization shows a superposition of all possible degenerate configurations, hence the spin orders along z show no order in the non-FM region, and the phase can only be identified by the strength of the x order. To confirm the existence of the unconventional non-FM phase, the spatial spin correlations are studied along z - x and z via exact diagonalization ($N = 12$) and VMC-SM on EPS ($N = 20$). Fig. 7 (a) presents the ev-

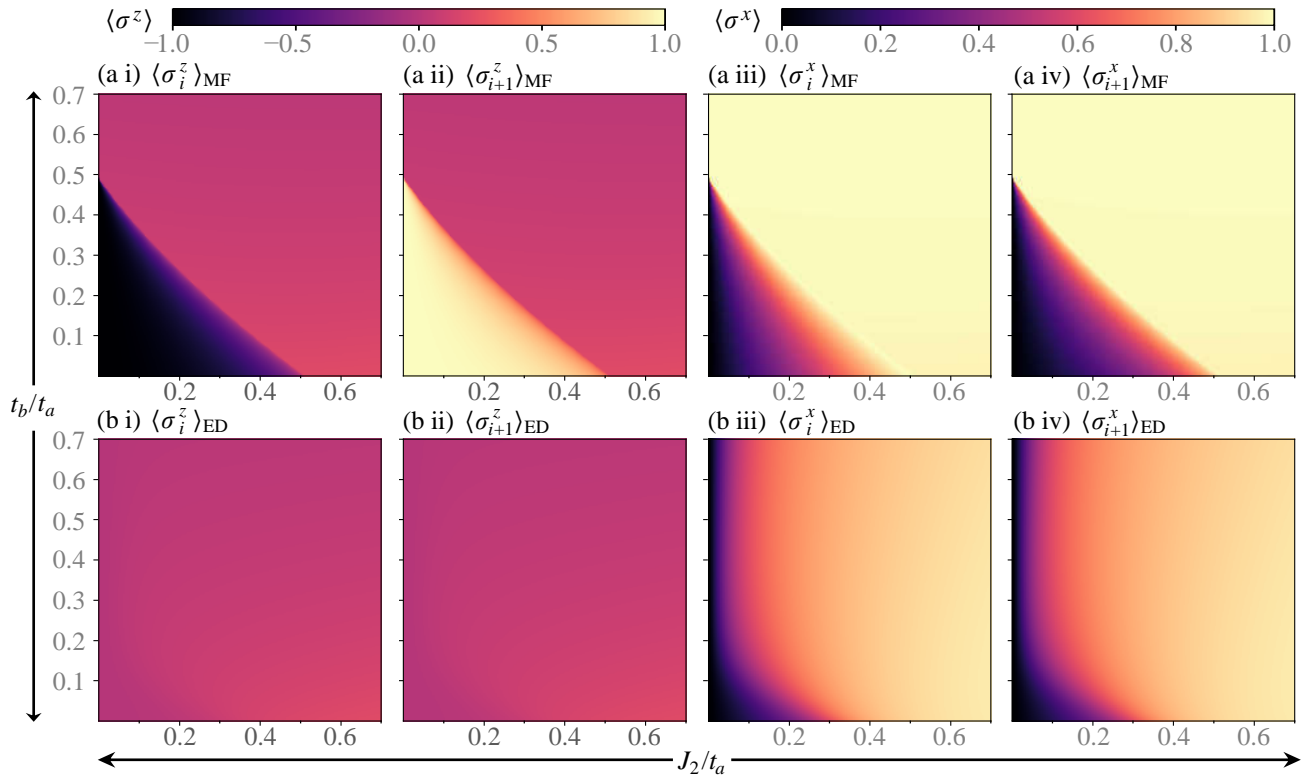


FIG. 4. (color online) Spin order parameters, describing the spin behavior along (i&ii) z and (iii&iv) x at site i in subspace A and $i+1$ in subspace B . The orders evaluated via (a) mean field approximation and (b) exact diagonalization for $N = 8$ are shown as a function of scaled tunneling (t_b/t_a) and coupling (J_2/t_a), in the deep Mott regime ($U/u_{ab} = 10, U_{ab}/t_a = 20$).

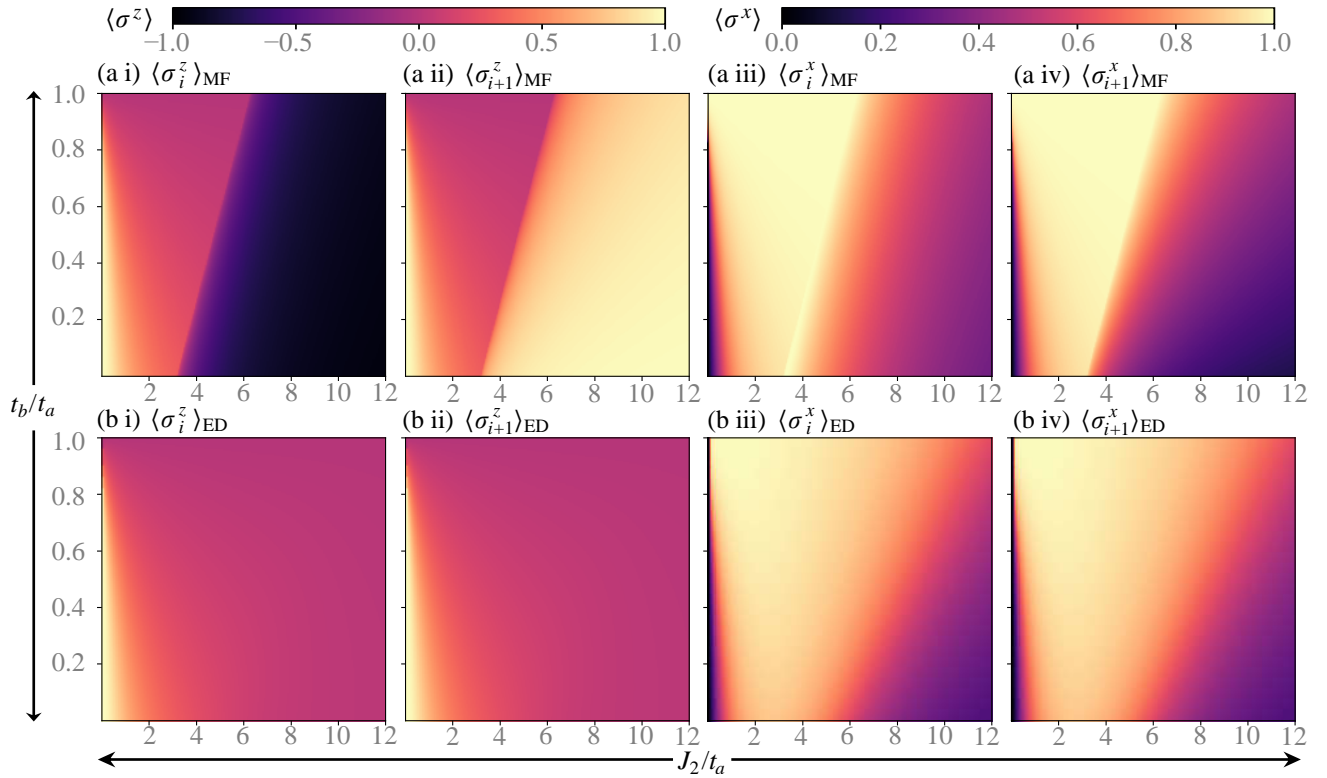


FIG. 5. (color online) Spin order parameters, as in Fig. 4, for $U/u_{ab} = 1.2$.

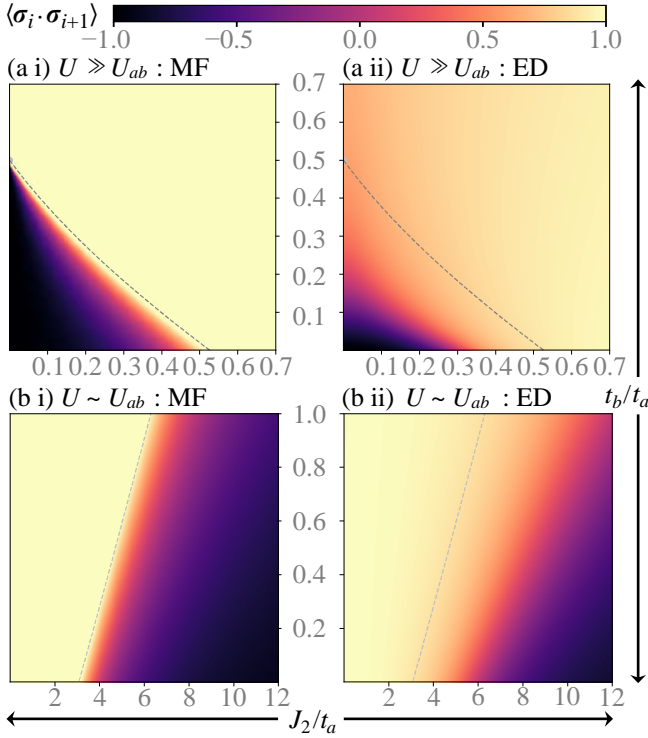


FIG. 6. (color online) Spin correlation describing the spin relationship between the neighboring sites at: (a) $U/U_{ab} = 10$ and (b) $U/U_{ab} = 1.2$ evaluated via (i) mean field approximation and (ii) exact diagonalization for $N = 8$. The correlation is shown as a function of scaled tunneling (t_b/t_a) and coupling (J_2/t_a), in the deep Mott regime ($U_{ab}/t_a = 20$). The dashed line denote the mean-field critical values (t_b/t_a)^C from Eqs. (5) and (6).

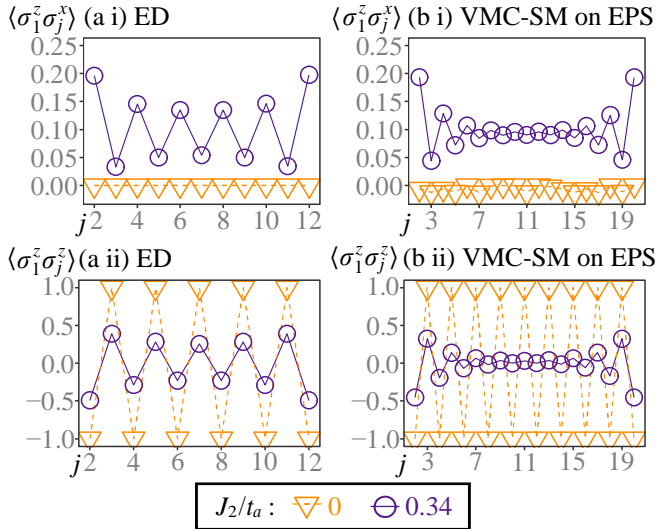


FIG. 7. (color online) Spin correlations describing the spin relationship between site 1 and some site j along: (i) z - x and (ii) z , for (a) $N = 12$ via exact diagonalization and (b) $N = 20$ via VMC-SM on EPS. The correlations are shown as a function of site j at $J_2/t_a = 0.34$, $t_b/t_a = 0.0$ and $J_2/t_a \approx 0.0$, $t_b/t_a = 0.0$ in the deep Mott regime ($U_{ab}/t_a = 20$, $U/U_{ab} = 10$).

idence of the unconventional site-dependent non-FM phase and a distinction between this and the conventional (z AFM) spin phase at different interaction limits, displaying spin correlations along z - x and z on site 1 and some site j obtained via exact diagonalization for system size $N = 12$ at $U \gg U_{ab}$. The unique correlations in the Hamiltonian manifests as oscillations in the spin correlations along z - x demonstrating a site-dependent behavior, whereas in the conventional regime the spin correlations remain constant as a function of site j . This oscillation in the spatial correlation acts as a signature of this unconventional non-FM phase, and an evidence of its existence in exact diagonalization. Similar oscillations appear for $U \sim U_{ab}$ but this phase behavior appears at large coupling regime ($J_2/t_a \sim 5$). The spin correlations are extended to a larger system size $N = 20$ to observe the decay in oscillation of the correlation in Fig. 7 (b).

VI. EXTENSION

In this section we discuss the effect of complex tunneling and coupling coefficients on the spin phases, and extend our study to comment on the effective spin system at occupancy greater than unity.

Complex coefficients: Complex phases are associated with the nearest-neighboring intra-component tunnelings t_a and t_b and the inter-component coupling J_2 resulting in new hopping parameters: $t_a = |t_a|e^{i\theta_a}$, $t_b = |t_b|e^{i\theta_b}$ and $J_2 = |J_2|e^{i\theta_J}$. The Hamiltonian for the resulting system:

$$H = - \sum_i (|t_a|e^{i\theta_a}a_i^\dagger a_{i+1} + |t_b|e^{i\theta_b}b_i^\dagger b_{i+1} + |J_2|e^{i\theta_J} + H.c.) + \sum_{k=a,b;i} \frac{U_k}{2} n_{ki}(n_{ki}-1) + \sum_i U_{ab} n_{ai} n_{bi} \quad (7)$$

The mapped effective spin Hamiltonian in the presence of complex coefficients:

$$H_{\text{eff}} = -J_z \sum_i \sigma_i^z \sigma_{i+1}^z - h_z \sum_i \sigma_i^z - J_p \sum_i [\cos(\theta_a - \theta_b)(\sigma_i^x \sigma_{i+1}^x + \sigma_i^y \sigma_{i+1}^y) + \sin(\theta_a - \theta_b)(\sigma_i^x \sigma_{i+1}^y - \sigma_i^y \sigma_{i+1}^x)] - h_x \sum_i [(t_a \cos(\theta_a - \theta_J) + t_b \cos(\theta_b - \theta_J))\sigma_i^x - (t_a \sin(\theta_a - \theta_J) + t_b \sin(\theta_b - \theta_J))\sigma_i^y] - J_{xz} \sum_i \cos(\theta_a - \theta_J)\sigma_i^x \sigma_{i+1}^z - \sin(\theta_a - \theta_J)\sigma_i^y \sigma_{i+1}^z + J_{zx} \sum_i \cos(\theta_b - \theta_J)\sigma_i^x \sigma_{i+1}^z - \sin(\theta_b - \theta_J)\sigma_i^y \sigma_{i+1}^z \quad (8)$$

The ferromagnetic ordering (J_p) of neighboring sites along x splits to x - x and x - y ordering and that along y splits to y - x

and y - y ordering. This splitting depends on the phase difference of coefficients t_a and t_b . However, the ordering J_z (along z) remains unchanged. The fictitious magnetic field (h_x) along x splits to x and y ; this splitting is dependent on the phase difference between tunneling (t_a or t_b) and coupling (J_2). The fictitious magnetic field (h_z) along z remains unchanged. A similar effect on the novel correlations with x - z (z - x) ordering on neighboring sites splitting to x - z and y - z (z - x and z - y) dependent on the phase difference of t_a or t_b and J_2 . The complex hopping parameters result in an accumulation of phase with each hop. In the case when a component hops to the neighboring site and back, there is no net phase accumulated, which results in the z ordering terms remaining unaffected. In any other hopping, a net phase is obtained, which is proportional to the difference of the complex phases associated with tunneling and coupling. Since this is a one-dimensional system, there is only a trivial effect of these complex coefficients; interesting outcomes are expected at higher dimensions.

Occupancy > 1: Considering two particles per site, the two-component Bose–Hubbard system is mapped to a spin-1 system with basis states $|aa\rangle$, $|ab\rangle$, and $|bb\rangle$ mapped to $|1\rangle$, $|0\rangle$, and $|-1\rangle$, respectively. Considering the limit $U \sim U_{ab}$, since only spin Mott phase ($|0\rangle$) persists for $U \gg U_{ab}$, the effective spin-1 Hamiltonian:

$$H_{\text{eff}} = \mu \sum_i (S_i^z)^2 - h_z^{(1)} \sum_i S_i^z - h_x^{(1)} \sum_i S_i^x - J_z \sum_i S_i^z S_{i+1}^z - J_p \sum_i (S_i^x S_{i+1}^x + S_i^y S_{i+1}^y) - J_{xz} \sum_i S_i^x S_{i+1}^z + J_{zx} \sum_i S_i^z S_{i+1}^x, \quad (9)$$

where S_i^α are the spin-1 matrices. $\mu = U - U_{ab}$ orders the sites along spin Mott ($|0\rangle$) phase for $\mu > 0$ and along z ($|1\rangle$ or $|-1\rangle$) for $\mu < 0$. Terms $h_z^{(1)} = 6(t_a^2 - t_b^2)/U_{ab}$ and $h_x^{(1)} = 6J_2(t_a + t_b)/U_{ab}$ act as fictitious magnetic fields polarizing the spins along z and x , respectively. Similar to spin-1/2, we note $J_p = 4t_a t_b/U_{ab}$ provides ferromagnetic ordering along x and y and $J_z = 4(t_a^2 + t_b^2 - J_2^2)/U_{ab}$ provides anti-ferromagnetic or ferromagnetic ordering along z (dependent on the tunneling and coupling parameters t_a , t_b , and J_2). $J_{xz} = 4J_2 t_a/U_{ab}$ and $J_{zx} = 4J_2 t_b/U_{ab}$ provide the novel ordering along x - z and z - x on nearest-neighboring sites. As expected, despite increasing the occupancy, the novel ordering persists. In spin-1, an additional competing parameter μ appears with an additional spin Mott phase.

Generalizing to spin $S = M/2$ for occupancy M , the effective spin- S Hamiltonian (S_i^α are spin S matrices) (Appendix D):

$$H_{\text{eff}} = \mu \sum_i (S_i^z)^2 - h_z^{(S)} \sum_i S_i^z - h_x^{(S)} \sum_i S_i^x - J_z \sum_i S_i^z S_{i+1}^z - J_p \sum_i (S_i^x S_{i+1}^x + S_i^y S_{i+1}^y) - J_{xz} \sum_i S_i^x S_{i+1}^z + J_{zx} \sum_i S_i^z S_{i+1}^x, \quad (10)$$

where $h_z^{(S)} = 2(2S+1)(t_a^2 - t_b^2)/U_{ab}$ and $h_x^{(S)} = 2(2S+1)J_2(t_a + t_b)/U_{ab}$.

VII. SUMMARY

In conclusion, coupling of the two components in the nearest-neighboring sites via a resonant two-photon Raman transition gives rise to new effective spin Hamiltonian and a unique site-dependent non-FM spin phase. The signature of this unique phase appears as oscillation in spatial z - x correlation between spins at site 1 and some site j , whereas it remains constant (~ 0) in a conventional z AFM spin phase. The phase space notably changes with the introduction of coupling, changing the previously seen first-order phase transition between the FM and non-FM (z AFM) spin phases to a second-order phase transition for $U \gg U_{ab}$. The transition width of this transition increases with J_2/t_a . For $U \sim U_{ab}$, the system goes from having only one (FM) spin phase to two phases (FM and non-FM) with a second-order phase transition between the two. Our analysis demonstrates that coupling of the components in the nearest neighboring sites provides an easily tunable parameter to switch between the previously seen z AFM, z FM and x FM spin phases allowing for the implementation of a spin independent optical lattice.

We employ exact diagonalization for small system size ($N \leq 12$) and Variational Monte Carlo with stochastic minimization on Entangled-Plaquette State for large system size ($N > 12$). These confirm the presence of strong unconventional correlations beyond the mean-field approximation. Introduction of complex intra-component tunneling and inter-component coupling alters the ordering along x . The unconventional correlations split to have x and y spin orders on a site and z on nearest-neighboring sites. For filling factor greater than unity, we present the effective spin Hamiltonian in the presence of coupling and demonstrate that the novel correlations persist, and also granting the possibility of transitioning between the different spin phases via the coupling instead of the on-site interactions.

Future Avenues: Our work provides new insights into the Bose–Hubbard model and offers an easily tunable phase parameter. The system with coupling can be investigated for symmetry protected topological (SPT) phases [100]. A possible extension to two tilted 1D optical lattices parallel to each other can obtain the SSH model and develop a SPT phase by tuning the coupling and tunneling parameters. Going to higher dimensions, new rich physics is expected [101]. Our assessment of the mapped system with complex hopping coefficients leads to the system acquiring a phase with second-order hopping. This is extensible to higher dimensions, where the phase acquired over hopping can have far more interesting consequences: development of Harper’s Hamiltonian [97] and interesting spin correlations in the mapped effective spin Hamiltonian. Additionally, the effect of the unconventional correlations for a generalized M occupancy at even and odd fillings using the mapped spin- $M/2$ Hamiltonian can be studied. In the absence of coupling, a spin-1 system mapped from two-component Bose–Hubbard model with occupancy two is used to lower entropy and obtain ultra-cold temperature [95]; this motivates the consideration of occupancy greater than one. The tunability of the system via coupling can provide additional control over the system at higher occupancy. Ryd-

berg atoms have garnered immense relevance for demonstrating interesting phases and system behavior with their long-range van der Waals interactions leading to blockade [102], and the resonant dipole-dipole interaction [100]. Finally, unexpected spin behaviors may emerge when incorporating Rydberg atoms on account of their interesting properties.

ACKNOWLEDGMENTS

This study was supported by the National Science Foundation under grant PHY-1912068 and the Welch Foundation under Grant No. C-1669.

Appendix A: Effective Hamiltonian: Canonical Transformation

Define two complementary subspaces: H_P (low-energy) with projector \mathcal{P} and H_Q (high-energy) with projector $\mathcal{Q}(=1-\mathcal{P})$. The effective Hamiltonian (up to second-order) can be expressed as [103]:

$$H_{\text{eff}} = \mathcal{P}H\mathcal{P} - \mathcal{P}H\mathcal{Q}\frac{1}{QH\mathcal{Q}}\mathcal{Q}H\mathcal{P} \quad (\text{A1})$$

The zeroth-order has no contribution as the hopping terms in the Hamiltonian lead to higher occupancy and are thus projected out. The interaction terms yield 0 for unit occupancy. In $\mathcal{P}H\mathcal{Q}$ or $\mathcal{Q}H\mathcal{P}$ the only contribution is from hopping terms (t_a, t_b, J_2) in the Hamiltonian that can couple the two subspaces. Whereas, in $\mathcal{Q}H\mathcal{Q}$, only the interaction terms (U, U_{ab}) contribute as they do not change the subspace. The second-order term is:

$$\begin{aligned} & \mathcal{P}H\mathcal{Q}\frac{1}{QH\mathcal{Q}}\mathcal{Q}H\mathcal{P} \\ &= \mathcal{P}\left(\sum_i (-t_a a_i^+ a_{i+1} - t_b b_i^+ b_{i+1} + h.c.) - J_2(b_i^+ a_{i+1} + a_{i+1}^+ b_i)\right)\mathcal{Q} \\ & \quad \left[\frac{1}{\mathcal{Q}(\sum_{k=a,b,i} \frac{U_k}{2} n_{ki}(n_{ki}-1) + \sum_i U_{ab} n_{ai} n_{bi})\mathcal{Q}}\right] \\ & \quad \mathcal{Q}\left(\sum_i (-t_a a_i^+ a_{i+1} - t_b b_i^+ b_{i+1} + h.c.) - J_2(b_i^+ a_{i+1} + a_{i+1}^+ b_i)\right)\mathcal{P} \end{aligned} \quad (\text{A2})$$

There are nine second-order or virtual hopping processes that contribute to and form the effective Hamiltonian. The first and second processes describe two particles of the same component exchanging positions. The eighth and ninth are processes when component b (or a) hops from $(i+1) \vee (i-1)$ to i and component a (or b) hops from i to $(i+1) \vee (i-1)$. These four processes have been studied previously [39] and result in the formation of $z\text{AFM}(\text{FM})$ and $xy\text{FM}$ phases. With the introduction of J_2 , five additional processes arise. The third process describes component a at $i+1$ and b at i exchanging positions. The fourth and sixth together represent

$(a \vee b)_{i,i+1} \rightarrow b_i, (a \vee b)_{i+1}$. Similarly, the fifth and seventh together describe $b_i, (a \vee b)_{i+1} \rightarrow (a \vee b)_{i,i+1}$. These processes are derived and expressed as follows:

$$\begin{aligned} \textcircled{1} & \frac{1}{QH\mathcal{Q}}\mathcal{P}\sum_i -t_a(a_{i+1}^+ + a_{i-1}^+)a_i\mathcal{Q}\sum_i -t_a a_i^+(a_{i+1} + a_{i-1})\mathcal{P} \\ &= \frac{t_a^2}{U_{ab}}\sum_i \mathcal{P}(n_{a,i+1} + n_{a,i-1})(a_i n_{b,i} a_i^+)\mathcal{P} \\ & \quad + \frac{t_a^2}{U}\sum_i \mathcal{P}(n_{a,i+1} + n_{a,i-1})(a_i(1 - n_{b,i})a_i^+)\mathcal{P} \\ &= \frac{t_a^2}{U_{ab}}\sum_i \left(\frac{I + \sigma_{i+1}^z}{2} + \frac{I + \sigma_{i-1}^z}{2}\right)\left(\frac{I - \sigma_i^z}{2}\right) \\ & \quad + \frac{t_a^2}{U}\sum_i \left(\frac{I + \sigma_{i+1}^z}{2} + \frac{I + \sigma_{i-1}^z}{2}\right)(I + \sigma_i^z) \\ &= \frac{t_a^2}{2U_{ab}}\sum_i (I - \sigma_i^z \sigma_{i+1}^z) + \frac{t_a^2}{U}\sum_i (I + 2\sigma_i^z + \sigma_i^z \sigma_{i+1}^z) \\ \textcircled{2} & \frac{1}{QH\mathcal{Q}}\mathcal{P}\sum_i -t_b(b_{i+1}^+ + b_{i-1}^+)b_i\mathcal{Q}\sum_i -t_b b_i^+(b_{i+1} + b_{i-1})\mathcal{P} \\ &= \frac{t_b^2}{2U_{ab}}\sum_i (I - \sigma_i^z \sigma_{i+1}^z) + \frac{t_b^2}{U}\sum_i (I - 2\sigma_i^z + \sigma_i^z \sigma_{i+1}^z) \\ \textcircled{3} & \frac{1}{QH\mathcal{Q}}\mathcal{P}\sum_i -J_2(a_{i+1}^+ b_i + b_{i-1}^+ a_i)\mathcal{Q}\sum_i -J_2(b_i^+ a_{i+1} + a_i^+ b_{i-1})\mathcal{P} \\ &= \frac{J_2^2}{QH\mathcal{Q}}\sum_i \mathcal{P}(n_{a,i+1} b_i \mathcal{Q} b_i^+ + n_{b,i-1} a_i \mathcal{Q} a_i^+)\mathcal{P} \\ &= \sum_i \left[\frac{J_2^2}{U} \mathcal{P} n_{a,i+1} (1 + n_{b,i}) (1 - n_{a,i}) + n_{b,i-1} (1 + n_{a,i}) (1 - n_{b,i}) \mathcal{P} + \right. \\ & \quad \left. \frac{J_2^2}{U_{ab}} \mathcal{P} n_{a,i+1} (1 + n_{b,i}) n_{a,i} + n_{b,i-1} (1 + n_{a,i}) n_{b,i} \mathcal{P} \right] \\ &= \frac{J_2^2}{U}\sum_i (I - \sigma_i^z \sigma_{i+1}^z) + \frac{J_2^2}{2U_{ab}}\sum_i (I + \sigma_i^z \sigma_{i+1}^z) \\ \text{The fourth and fifth processes together contribute to the fictitious magnetic field } h_x \text{ and novel correlation } J_{xz}. \\ \textcircled{4} & \frac{1}{QH\mathcal{Q}}\mathcal{P}\sum_i -t_a(a_{i+1}^+ + a_{i-1}^+)a_i\mathcal{Q}\sum_i -J_2(b_i^+ a_{i+1} + a_i^+ b_{i-1})\mathcal{P} \\ &= \frac{J_2 t_a}{U_{ab}}\sum_i \mathcal{P}(n_{a,i+1} b_i^+ a_i + a_{i-1}^+ b_{i-1} a_i n_{b,i} a_i^+)\mathcal{P} \\ & \quad + \frac{J_2 t_a}{U}\sum_i \mathcal{P} a_{i-1}^+ b_{i-1} a_i (1 - n_{b,i}) a_i^+ \mathcal{P} \\ &= \frac{J_2 t_a}{2U_{ab}}\sum_i (\sigma_i^x - i\sigma_i^y \sigma_{i+1}^z) \\ & \quad + \frac{J_2 t_a}{2U}\sum_i (\sigma_{i-1}^x + i\sigma_{i-1}^y + \sigma_i^z \sigma_{i-1}^x + i\sigma_i^z \sigma_{i-1}^y) \end{aligned}$$

$$\begin{aligned}
⑤ & \frac{1}{QH\bar{Q}} \mathcal{P} \sum_i -J_2 (a_{i+1}^+ b_i + b_{i-1}^+ a_i) \bar{Q} \sum_i -t_a a_i^+ (a_{i+1} + a_{i-1}) \mathcal{P} \\
&= \frac{J_2 t_a}{QH\bar{Q}} \sum_i \mathcal{P} (n_{a,i+1} b_i Q a_i^+ + b_{i-1}^+ a_{i-1} Q a_i^+) \mathcal{P} \\
&= \frac{J_2 t_a}{2U_{ab}} \sum_i (\sigma_i^x + i\sigma_i^y \sigma_{i+1}^z) \\
&\quad + \frac{J_2 t_a}{2U} \sum_i (\sigma_{i-1}^x - i\sigma_{i-1}^y + \sigma_i^z \sigma_{i-1}^x - i\sigma_i^z \sigma_{i-1}^y)
\end{aligned}$$

The sixth and seventh processes together contribute to the fictitious magnetic field h_x and novel correlation J_{zx} .

$$\begin{aligned}
⑥ & \frac{1}{QH\bar{Q}} \mathcal{P} \sum_i -t_b (b_{i+1}^+ + b_{i-1}^+) b_i \bar{Q} \sum_i -J_2 (b_i^+ a_{i+1} + a_i^+ b_{i-1}) \mathcal{P} \\
&= \frac{J_2 t_b}{QH\bar{Q}} \sum_i \mathcal{P} (n_{b,i-1} b_i Q a_i^+ + b_{i+1}^+ a_{i+1} b_i Q b_i^+) \mathcal{P} \\
&= \frac{J_2 t_b}{2U_{ab}} \sum_i (\sigma_i^x - i\sigma_i^y \sigma_{i-1}^z) \\
&\quad + \frac{J_2 t_b}{2U} \sum_i \sigma_{i+1}^x - i\sigma_{i+1}^y - \sigma_i^z \sigma_{i+1}^x + i\sigma_i^z \sigma_{i+1}^y
\end{aligned}$$

$$\begin{aligned}
⑦ & \frac{1}{QH\bar{Q}} \mathcal{P} \sum_i -J_2 (a_{i+1}^+ b_i + b_{i-1}^+ a_i) \bar{Q} \sum_i -t_b b_i^+ (b_{i+1} + b_{i-1}) \mathcal{P} \\
&= \frac{J_2 t_b}{QH\bar{Q}} \sum_i \mathcal{P} (n_{b,i-1} a_i Q b_i^+ + a_{i+1}^+ b_{i+1} b_i Q b_i^+) \mathcal{P} \\
&= \frac{J_2 t_b}{2U_{ab}} \sum_i (\sigma_i^x + i\sigma_i^y \sigma_{i-1}^z) \\
&\quad + \frac{J_2 t_b}{2U} \sum_i \sigma_{i+1}^x + i\sigma_{i+1}^y - \sigma_i^z \sigma_{i+1}^x - i\sigma_i^z \sigma_{i+1}^y
\end{aligned}$$

$$\begin{aligned}
⑧ & \frac{1}{QH\bar{Q}} \mathcal{P} \sum_i -t_a (a_{i+1}^+ + a_{i-1}^+) a_i \bar{Q} \sum_i -t_b b_i^+ (b_{i+1} + b_{i-1}) \mathcal{P} \\
&= \frac{t_a t_b}{4U_{ab}} \sum_i \left[(\sigma_{i+1}^x + i\sigma_{i+1}^y) (\sigma_i^x - i\sigma_i^y) + (\sigma_{i-1}^x + i\sigma_{i-1}^y) (\sigma_i^x - i\sigma_i^y) \right] \\
&= \frac{t_a t_b}{2U_{ab}} \sum_i (\sigma_i^x \sigma_{i+1}^x + \sigma_i^y \sigma_{i+1}^y) \\
⑨ & \frac{1}{QH\bar{Q}} \mathcal{P} \sum_i -t_b (b_{i+1}^+ + b_{i-1}^+) b_i \bar{Q} \sum_i -t_a a_i^+ (a_{i+1} + a_{i-1}) \mathcal{P} \\
&= \frac{t_a t_b}{2U_{ab}} \sum_i (\sigma_i^x \sigma_{i+1}^x + \sigma_i^y \sigma_{i+1}^y)
\end{aligned}$$

Then, the second term ($\mathcal{P} H \bar{Q} \bar{Q} H \mathcal{P}$) in the expansion A1:

$$\begin{aligned}
&= \frac{t_a t_b}{U_{ab}} \sum_i (\sigma_i^x \sigma_{i+1}^x + \sigma_i^y \sigma_{i+1}^y) + (t_a^2 + t_b^2 - J_2^2) \left(\frac{1}{U} - \frac{1}{2U_{ab}} \right) \sum_i \sigma_i^z \sigma_{i+1}^z \\
&\quad + 2 \frac{t_a^2 - t_b^2}{U} \sum_i \sigma_i^z + J_2 (t_a + t_b) \left(\frac{1}{U} + \frac{1}{U_{ab}} \right) \sum_i \sigma_i^x \\
&\quad - \frac{J_2 t_b}{U} \sum_i \sigma_i^z \sigma_{i+1}^x + \frac{J_2 t_a}{U} \sum_i \sigma_i^x \sigma_{i+1}^z
\end{aligned} \tag{A3}$$

Finally, the effective spin Hamiltonian is:

$$\begin{aligned}
H_{\text{eff}} = \sum_i & \left[-J_{\perp} (\sigma_i^x \sigma_{i+1}^x + \sigma_i^y \sigma_{i+1}^y) - J_z \sigma_i^z \sigma_{i+1}^z - h_z (\sigma_i^z) \right. \\
& \left. - h_x (\sigma_i^x) + J_{zx} \sigma_i^z \sigma_{i+1}^x - J_{xz} \sigma_i^x \sigma_{i+1}^z \right] \tag{A4}
\end{aligned}$$

Appendix B: N = 2

The aim here is to investigate a simplified two-site system as it provides a facile description allowing for the validation of the effective spin system, by comparing the ground states of the original with the mapped two-component Bose-Hubbard Hamiltonian. Consider two sites each hosting component $a \vee b$, forming the basis states $|a\rangle_1 |a\rangle_2, |a\rangle_1 |b\rangle_2, |b\rangle_1 |a\rangle_2$ and $|b\rangle_1 |b\rangle_2$ with the analysis restricted to the limits $U \gg U_{ab}$ and $U \sim U_{ab}$. The coupling and the tunneling couples these basis states in the original system to high-energy states $|aa\rangle_1 |0\rangle_2, |0\rangle_1 |aa\rangle_2, |ab\rangle_1 |0\rangle_2, |0\rangle_1 |ab\rangle_2, |bb\rangle_1 |0\rangle_2$ and $|0\rangle_1 |bb\rangle_2$. The effective spin Hamiltonian and the original Hamiltonian are studied via exact diagonalization with open boundary conditions. In Fig. 8, the ground state of the mapped effective spin system is presented as a function of coupling (J/t_a) and tunneling (t_b/t_a). Upon comparison of the mapped spin system with the ground state of the original system in Fig. 9 (low-energy subspace), both systems show a similar ground state composition as a function of tunneling and coupling. At large coupling ($J/t_a \gg t_b/t_a$) the ground state compositions of the two systems deviate, where the mapped system shows a lower probability of the state $|b\rangle_1 |a\rangle_2$ and thus higher probability of the other three basis states. At higher values of coupling, the Mott condition required for the mapping fails, leading to a negligible but non-zero probability of high energy states $|aa\rangle_1 |0\rangle_2, |0\rangle_1 |aa\rangle_2, |ab\rangle_1 |0\rangle_2, |0\rangle_1 |ab\rangle_2, |bb\rangle_1 |0\rangle_2$ and $|0\rangle_1 |bb\rangle_2$ in the ground state of the original Hamiltonian as seen in Fig. 10 (high-energy subspace). Additionally, the mapped effective Hamiltonian works best for a large system size and in the derivation of the effective Hamiltonian the expansion is limited to second-order; inclusion of higher order terms can reduce the deviation seen in the ground state composition between the mapped and original system. Studying the probability of basis states, we confirm that the mapped system is an appropriate representation for the parameter strengths considered. We explain the ground state of mapped system by studying the effective Hamiltonian. The preference for $|b\rangle_1 |a\rangle_2$ appears due to $J_z \propto J_2$, and for $|a\rangle_1 |a\rangle_2$ or $|b\rangle_1 |b\rangle_2$ due to $J_z, h_z \propto t_{a \vee b}$ ordering, whereas the preference for the superposition of states $|a\rangle_1 |a\rangle_2$ and $|b\rangle_1 |a\rangle_2$ or $|b\rangle_1 |b\rangle_2$ and $|b\rangle_1 |a\rangle_2$ emerges due to J_{zx} or J_{xz} .

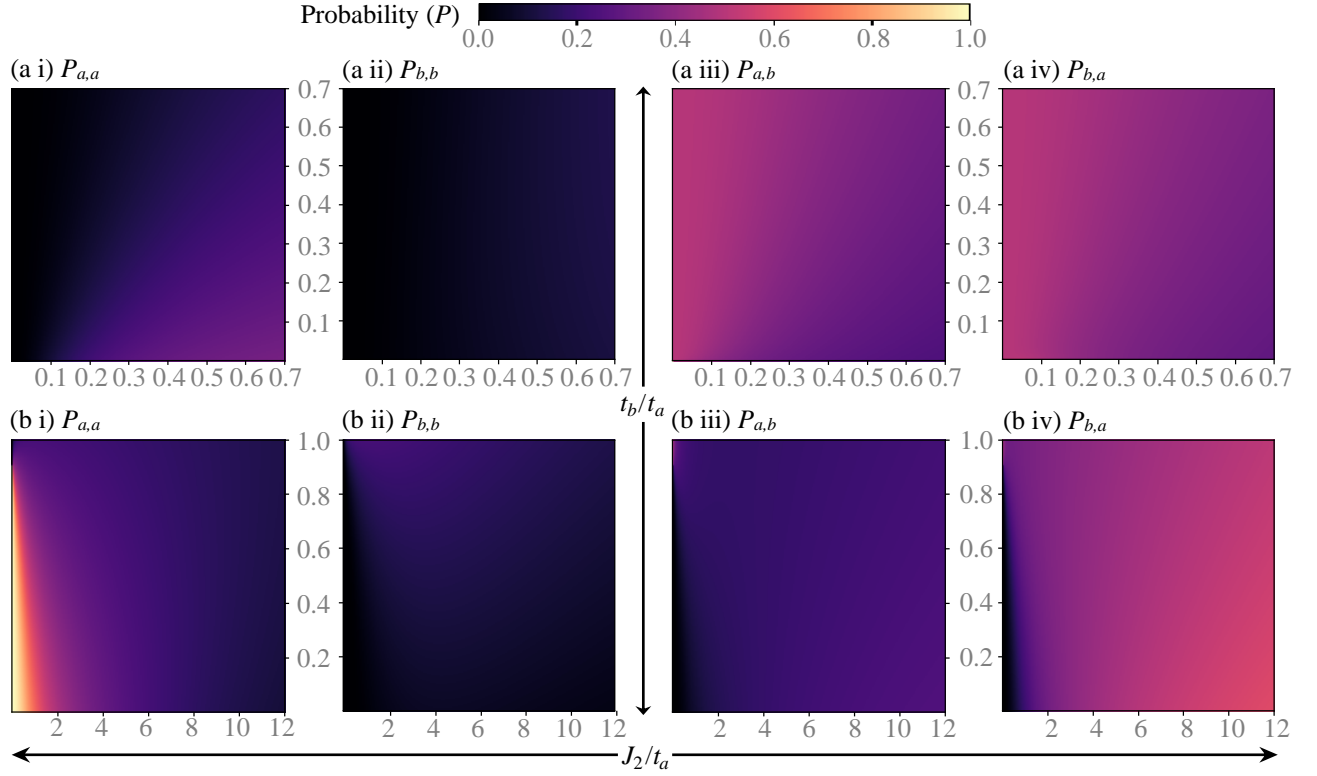


FIG. 8. (color online) Probability of the basis states of the effective Hamiltonian (i) $|a\rangle_1|a\rangle_2$, (ii) $|b\rangle_1|b\rangle_2$, (iii) $|a\rangle_1|b\rangle_2$, and (iv) $|b\rangle_1|a\rangle_2$. The probabilities are determined in the deep Mott regime ($U_{ab}/t_a = 20$) (a) $U/U_{ab} = 10$ and (b) $U/U_{ab} = 1.2$ and presented as a function of scaled tunneling (t_b/t_a) and coupling (J_2/t_a).

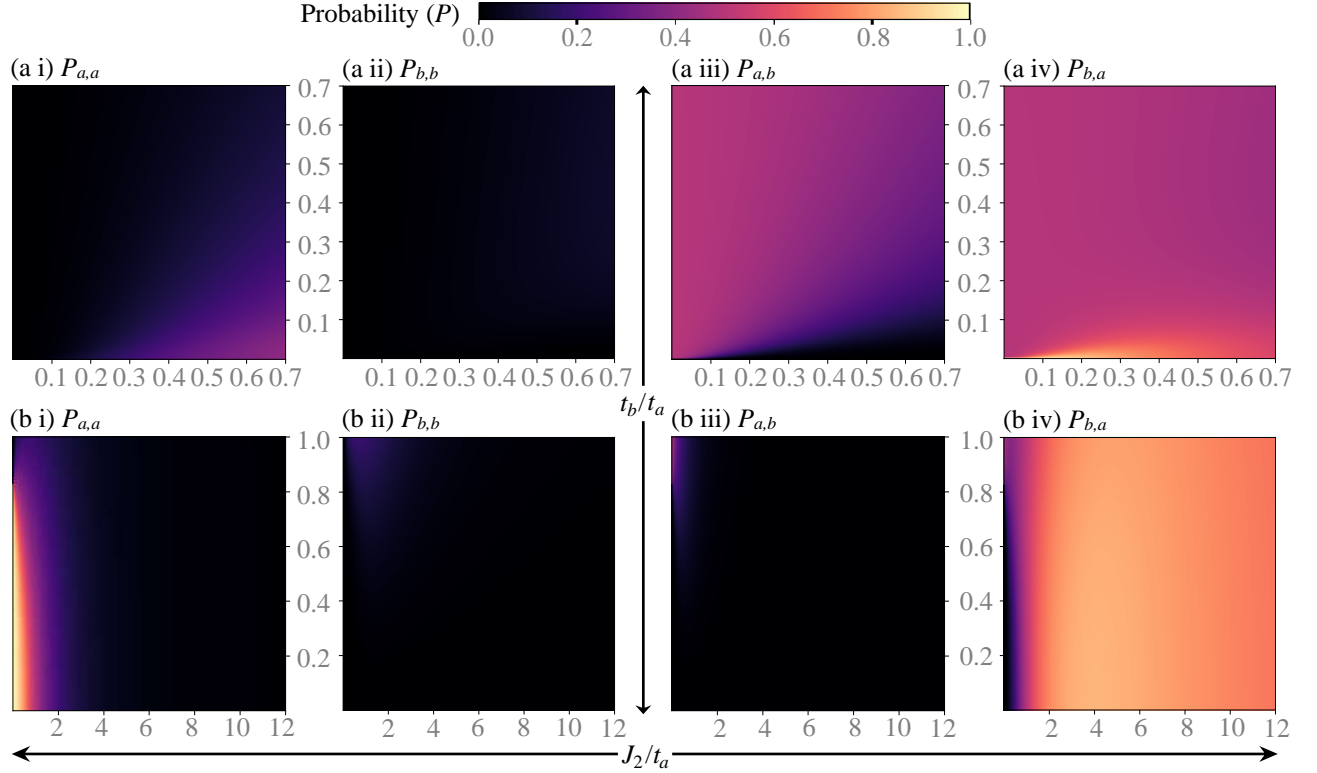


FIG. 9. (color online) Probability of the low-energy basis states of the original Hamiltonian, as in Fig. 8.

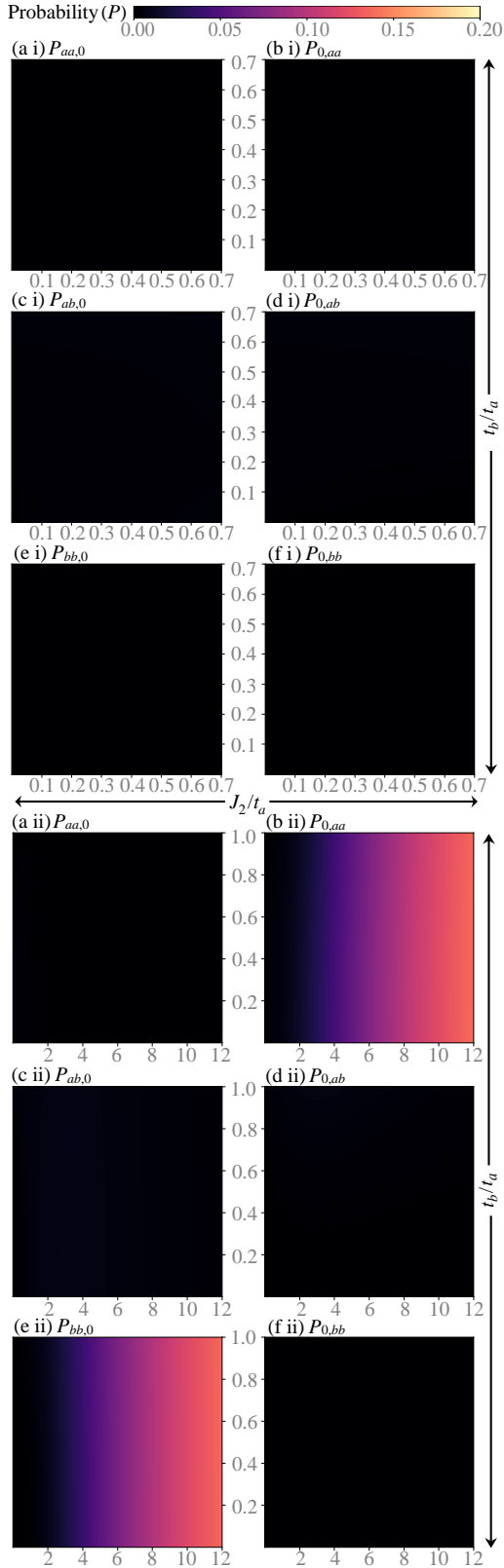


FIG. 10. (color online) Probability of the high-energy basis states of the original Hamiltonian (a) $|aa\rangle_1|0\rangle_2$, (b) $|0\rangle_1|aa\rangle_2$, (c) $|ab\rangle_1|0\rangle_2$, (d) $|0\rangle_1|ab\rangle_2$, (e) $|bb\rangle_1|0\rangle_2$, and (f) $|0\rangle_1|bb\rangle_2$. The probabilities are determined in the deep Mott regime (i) $U/U_{ab} = 10$ or (ii) $U/U_{ab} = 1.2$, $U_{ab}/t_a = 20$ and presented as a function of scaled tunneling (t_b/t_a) and coupling (J_2/t_a).

Appendix C: Analytical Phase Boundary

Within the mean field approximation, with the variational ansatz defined, the energy per site:

$$E_{MF} = -J_z \cos 2\theta_A \cos 2\theta_B - J_p \sin 2\theta_A \sin 2\theta_B - \frac{h_z}{2} (\cos 2\theta_A + \cos 2\theta_B) - \frac{h_x}{2} (\sin 2\theta_A + \sin 2\theta_B) - \frac{(J_{xz} - J_{zx})}{2} (\cos 2\theta_A \sin 2\theta_B + \sin 2\theta_A \cos 2\theta_B)$$

Minimizing energy with respect to θ_B ($\partial E / \partial \theta_B = 0$):

$$\sin 2\theta_B = \frac{K_1}{\sqrt{K_1^2 + K_2^2}}, \quad \cos 2\theta_B = \frac{K_2}{\sqrt{K_1^2 + K_2^2}},$$

where $K_1 = J_p \sin 2\theta_A + \frac{(J_{xz} - J_{zx})}{2} \cos 2\theta_A + \frac{h_x}{2}$ and

$$K_2 = J_z \cos 2\theta_A + \frac{(J_{xz} - J_{zx})}{2} \sin 2\theta_A + \frac{h_z}{2}.$$

Energy after eliminating θ_B :

$$E_{MF} = -\frac{1}{2} (h_z \cos 2\theta_A + h_x \sin 2\theta_A) - \sqrt{K_1^2 + K_2^2}$$

The energy is too complicated to solve for θ_A , approximations are made to obtain analytical expressions for θ_A .

$U \gg U_{ab}$: We consider two approximations. In approximation (i), consider only J_p, J_z and h_x . This is valid for small and intermediate t_b/t_a and J_2/t_a . Under this assumption, the non-FM phase is approximately captured:

$$E_{MF} = -\frac{h_x \sin 2\theta_A}{2} - \sqrt{(J_z^2 - J_p^2) \cos^2 2\theta_A + J_p h_x \sin 2\theta_A + J_p^2 + \frac{h_x^2}{4}}$$

Minimizing energy with respect to θ_A and solving for θ_A :

$$\sin 2\theta_A^{NFM,1\vee 2} = \frac{J_p h_x \pm |J_z| h_x}{2(J_z^2 - J_p^2)}$$

$$\sin 2\theta_A^{NFM,3} = 1$$

$\theta_A^{NFM,1}$ fits the numerically obtained θ_A best among the three in the non-FM region.

In approximation (ii), consider each of the following cases:

1. J_z, h_x (large J_2/t_a and small t_b/t_a) or
2. J_p, J_z (small J_2/t_a and large t_b/t_a) or
3. J_p, h_x (large J_2/t_a and large t_b/t_a),

where the terms are significant. In all of the three cases:

$$\cos 2\theta_A^{FM} = 0$$

The critical value of t_b/t_a , going from non-FM to FM, obtained by finding the boundary between the two analytical θ_A is computed:

$$(t_b/t_a)_{U \gg U_{ab}}^C = -\left(\frac{J_2/t_a(U+U_{ab})+2U}{2(2U_{ab}-U)}\right) - \sqrt{\left(\frac{J_2/t_a(U+U_{ab})+2U}{2(2U_{ab}-U)}\right)^2 - \left(1 - J_2^2/t_a^2 + \frac{J_2/t_a(U+U_{ab})}{2U_{ab}-U}\right)}$$

$U \sim U_{ab}$: We consider two approximations. In approximation (i), set h_z and $J_{xz} - J_{zx}$ to 0. This is valid when the intra-component tunnelings are small ($t_b, t_a \ll J_2$), or comparable to each other ($t_a \sim t_b$). This limit is able to approximately capture the non-FM phase.

$$E_{MF} = -\frac{h_x \sin 2\theta_A}{2} - \sqrt{(J_z^2 - J_p^2) \cos^2 2\theta_A + J_p h_x \sin 2\theta_A + J_p^2 + \frac{h_x^2}{4}}$$

Minimizing energy with respect to θ_A and solving for θ_A :

$$\sin 2\theta_A^{NFM,1 \vee 2} = \frac{J_p h_x \pm |J_z| h_x}{2(J_z^2 - J_p^2)}$$

$$\sin 2\theta_A^{NFM,3} = 1$$

$\theta_A^{NFM,1}$ fits the numerically obtained θ_A best among the three in the non-FM region.

In approximation (ii), set J_z , J_p and $J_{xz} - J_{zx}$ to 0. This solution set only considers the spin polarizing terms h_z and h_x , and is able to capture the FM phase. This approximation is valid for small coupling J_2/t_a . It however fails to capture the region around $t_b/t_a \sim 1$ and $J_2/t_a \rightarrow 0$, where both the ordering terms considered would tend to 0.

$$E_{MF} = -\frac{h_z \cos 2\theta_A}{2} - \frac{h_x \sin 2\theta_A}{2} - \sqrt{\frac{h_z^2 + h_x^2}{4}}$$

Minimizing energy with respect to θ_A and solving for θ_A

$$\cos 2\theta_A^{FM} = \frac{h_z}{\sqrt{h_z^2 + h_x^2}}$$

The critical value of t_b/t_a , going from non-FM to FM, obtained by finding the boundary between the two analytical θ_A is computed ($\theta_A^{NFM,1} = \lim_{h_z \rightarrow 0} \theta_A^{FM} = \pi/4$):

$$(t_b/t_a)_{U \sim U_{ab}}^C = -\left(\frac{J_2/t_a(U+U_{ab})+2U}{2(2U_{ab}-U)}\right) + \sqrt{\left(\frac{J_2/t_a(U+U_{ab})+2U}{2(2U_{ab}-U)}\right)^2 - \left(1 - J_2^2/t_a^2 + \frac{J_2/t_a(U+U_{ab})}{2U_{ab}-U}\right)}$$

Appendix D: Mapping M particles per site

Generalizing the system to M particles per site, with the analysis limited to $U - U_{ab} = \mu \ll U, U_{ab}$, consider a site having n_a particles of component a and n_b of component b , such that $n_a + n_b = M$. To map the two-component Bose-Hubbard model to an effective low-energy Hamiltonian, define the subspaces P (occupancy = M) and Q (occupancy $> M$).

The effective Hamiltonian up to second-order:

$$H_{\text{eff}} = PHP - PHQ \frac{1}{QHQP - PHP} QHP$$

Mapping the bosonic creation, annihilation, and number operators to Spin $M/2$ matrices:

$$n_{a,i} = \frac{M}{2} + S_i^z, \quad n_{b,i} = \frac{M}{2} - S_i^z$$

$$a_i^\dagger b_i = S_i^x + iS_i^y, \quad b_i^\dagger a_i = S_i^x - iS_i^y$$

First term in the Hamiltonian:

$$PHP = \frac{U}{2} n_{a,i}(n_{a,i}-1) + \frac{U}{2} n_{b,i}(n_{b,i}-1) + U_{ab} n_{a,i} n_{b,i}$$

$$= \frac{U}{2} M(M-1) - \mu \frac{M^2}{4} + \mu (S_i^z)^2$$

Second term in the Hamiltonian, $-PHQ \frac{1}{QHQP - PHP} QHP$, is split into 4 terms:

$$(a) -t_a^2 P \left[(n_{a,i+1} + n_{a,i-1}) a_i \frac{Q}{QHQP - PHP} a_i^\dagger \right] P$$

$$-t_b^2 P \left[(n_{b,i+1} + n_{b,i-1}) b_i \frac{Q}{QHQP - PHP} b_i^\dagger \right] P$$

$$-J_2^2 P \left[n_{a,i+1} b_i \frac{Q}{QHQP - PHP} b_i^\dagger + n_{b,i-1} a_i \frac{Q}{QHQP - PHP} a_i^\dagger \right] P$$

$$(b) -t_a t_b P \left[(a_{i+1}^\dagger b_{i+1} + a_{i-1}^\dagger b_{i-1}) a_i \frac{Q}{QHQP - PHP} b_i^\dagger \right. \\ \left. + (b_{i+1}^\dagger a_{i+1} + b_{i-1}^\dagger a_{i-1}) b_i \frac{Q}{QHQP - PHP} a_i^\dagger \right] P$$

$$(c) -J_2 t_a P \left[n_{a,i+1} \left(a_i \frac{Q}{QHQP - PHP} b_i^\dagger + b_i \frac{Q}{QHQP - PHP} a_i^\dagger \right) \right. \\ \left. + (a_{i-1}^\dagger b_{i-1} + b_{i-1}^\dagger a_{i-1}) a_i \frac{Q}{QHQP - PHP} a_i^\dagger \right] P$$

$$(d) -J_2 t_b P \left[n_{b,i-1} \left(a_i \frac{Q}{QHQP - PHP} b_i^\dagger + b_i \frac{Q}{QHQP - PHP} a_i^\dagger \right) \right. \\ \left. + (a_{i+1}^\dagger b_{i+1} + b_{i+1}^\dagger a_{i+1}) b_i \frac{Q}{QHQP - PHP} b_i^\dagger \right] P$$

Focusing on (a), $QHQP - PHP \approx U_{ab} M$; $a_i Q a_i^\dagger$

$$= \sum_{n_b=0}^M a_i \left[\prod_{k=0, k \neq n_b}^N \frac{(k - n_{b,i})}{(k - n_b)} \right] a_i^\dagger = \sum_{n_b=0}^M (n_a + 1) \left[\prod_{k=0, k \neq n_b}^N \frac{(k - n_{b,i})}{(k - n_b)} \right]$$

$$\begin{aligned}
&= \sum_{n_b=0}^M (M+1-n_b) \left[\frac{1}{n_b!} \frac{1}{(M-n_b)!} \right] \left[(-1)^{n_b} \prod_{k=0, k \neq n_b}^M (k-n_{b,i}) \right] \\
&= \frac{1}{M!} \sum_{n_b=0}^M (-1)^{n_b} (M+1-n_b) \binom{M}{n_b} \left[\prod_{k=0, k \neq n_b}^M (k-n_{b,i}) \right] \\
b_i Q b_i^+ &= \frac{1}{M!} \sum_{n_a=0}^M (-1)^{n_a} (M+1-n_a) \binom{M}{n_a} \left[\prod_{k=0, k \neq n_a}^M (k-n_{a,i}) \right]
\end{aligned}$$

Simplification of the terms in the above expression:

$$\begin{aligned}
\prod_{k=0, k \neq n_b}^M (k-n_{b,i}) &= C_0 + C_1 n_{b,i} + C_2 n_{b,i}^2 + \dots + C_M n_{b,i}^M \\
C_M &= (-1)^M \\
C_{M-1} &= (-1)^M n_b + (-1)^{M-1} (\sum_{n_1=0}^M n_1), \\
C_{M-2} &= (-1)^M n_b^2 + (-1)^{M-1} (\sum_{n_1=0}^M n_1) n_b \\
&\quad + (-1)^{M-2} (\sum_{n_1=0}^M \sum_{n_2 > n_1} n_1 n_2) + \dots \\
C_1 &= (-1)^M n_b^{M-1} + \dots, \\
C_0 &= (-1)^M n_b^M + (-1)^{M-1} (\sum_{n_1=0}^M n_1) n_b^{M-1} + \dots \\
C_{M-k} &= (-1)^M n_b^k + (-1)^{M-1} (\sum_{n_1=0}^M n_1) n_b^{k-1} + \dots \\
\sum_{n_b} (-1)^{n_b} n_b^k \binom{M}{n_b} &= \begin{cases} (-1)^M M!, & \text{if } k = M \\ 0, & k < M \end{cases} \\
n_b^M &= n_b(n_b-1)(n_b-2)\dots(n_b-(M-1)) + (\sum_{n_1=0}^{M-1} n_1) n_b^{M-1}
\end{aligned}$$

Substituting these simplifications: $a_i Q a_i^+$

$$\begin{aligned}
&= \frac{1}{M!} \sum_{n_b=0}^M (-1)^{n_b} (M+1-n_b) \binom{M}{n_b} \left[\prod_{k=0, k \neq n_b}^M (k-n_{b,i}) \right] \\
&= \frac{1}{M!} \sum_{n_b=0}^M (M+1) (-1)^{n_b} \binom{M}{n_b} (-1)^M n_b^M \\
&\quad - \frac{1}{M!} \sum_{n_b=0}^M n_b (-1)^{n_b} \binom{M}{n_b} \left((-1)^M n_b^M + (-1)^{M-1} \left(\sum_{n=0}^M n \right) n_b^{M-1} \right. \\
&\quad \left. + (-1)^M n_b^{M-1} n_{b,i} \right) \\
&= (M+1) - n_{b,i} - \frac{1}{M!} \sum_{n_b=0}^M (-1)^{n_b} \binom{M}{n_b} \left((-1)^M n_b n_b (n_b-1) \dots \right. \\
&\quad \left. \dots (n_b - (M-1)) + (-1)^M \left(\sum_{n=0}^{M-1} n \right) n_b^M + (-1)^{M-1} \left(\sum_{n=0}^M n \right) n_b^M \right) \\
&= (M+1) - n_{b,i} - M \\
&\quad - \frac{1}{M!} \sum_{n_b=0}^M (-1)^{n_b} \binom{M}{n_b} (-1)^M \left(\frac{M(M-1)}{2} - \frac{M(M+1)}{2} \right) n_b^M \\
&= (M+1) - n_{b,i} - M + M = (M+1) - n_{b,i} \\
b_i Q b_i^+ &= (M+1) - n_{a,i}
\end{aligned}$$

Simplifying (a) in the expression:

(z: number of nearest neighbors)

$$\begin{aligned}
(a) &= -\frac{t_a^2}{MU_{ab}} P[(n_{a,i+1} + n_{a,i-1})(M+1-n_{b,i})] P \\
&\quad - \frac{t_b^2}{MU_{ab}} P[(n_{b,i+1} + n_{b,i-1})(M+1-n_{a,i})] P \\
&\quad - \frac{J_2^2}{MU_{ab}} P[n_{b,i+1}(M+1-n_{b,i}) + n_{a,i-1}(M+1-n_{a,i})] P \\
&= -\frac{z t_a^2}{MU_{ab}} (\text{Const.} + (M+1) S_i^z + S_i^z S_{i+1}^z) \\
&\quad - \frac{z t_b^2}{MU_{ab}} (\text{Const.} - (M+1) S_i^z + S_i^z S_{i+1}^z) + \frac{z J_2^2}{MU_{ab}} S_i^z S_{i+1}^z
\end{aligned}$$

Considering the other terms in the second expression of the Effective Hamiltonian: (For (b), (c), and (d), $QHQP-PHP \approx U/2(M-1) + U_{ab}/2(M+1) \approx U_{ab}M$):

$$\begin{aligned}
(b) &= -t_a t_b P \left[(a_{i+1}^+ b_{i+1} + a_{i-1}^+ b_{i-1}) a_i \frac{Q}{QHQP-PHP} b_i^+ \right. \\
&\quad \left. + (b_{i+1}^+ a_{i+1} + b_{i-1}^+ a_{i-1}) b_i \frac{Q}{QHQP-PHP} a_i^+ \right] P \\
&= -\frac{t_a t_b}{MU_{ab}} P \left[(a_{i+1}^+ b_{i+1} + a_{i-1}^+ b_{i-1}) a_i \left(\sum_{n_a} \prod_{k=0, k \neq n_a}^M \frac{(k-n_{a,i})}{(k-n_a)} \right) b_i^+ \right. \\
&\quad \left. + (b_{i+1}^+ a_{i+1} + b_{i-1}^+ a_{i-1}) b_i \left(\sum_{n_b} \prod_{k=0, k \neq n_b}^M \frac{(k-n_{b,i})}{(k-n_b)} \right) a_i^+ \right] P \\
&= -\frac{t_a t_b}{MU_{ab}} P \left[(a_{i+1}^+ b_{i+1} + a_{i-1}^+ b_{i-1}) b_i^+ a_i \frac{M!}{M!} \right. \\
&\quad \left. + (b_{i+1}^+ a_{i+1} + b_{i-1}^+ a_{i-1}) a_i^+ b_i \frac{M!}{M!} \right] P \\
&= -\frac{z t_a t_b}{MU_{ab}} ((S_{i+1}^x + i S_{i+1}^y)(S_i^x - i S_i^y) + (S_{i+1}^x - i S_{i+1}^y)(S_i^x + i S_i^y)) \\
&= -\frac{z 2 t_a t_b}{MU_{ab}} (S_i^x S_{i+1}^x + S_i^y S_{i+1}^y) \\
(c) &= -J_2 t_a P \left[n_{a,i+1} \left(a_i \frac{Q}{QHQP-PHP} b_i^+ + b_i \frac{Q}{QHQP-PHP} a_i^+ \right) \right. \\
&\quad \left. + (a_{i-1}^+ b_{i-1} + b_{i-1}^+ a_{i-1}) a_i \frac{Q}{QHQP-PHP} a_i^+ \right] P \\
&= -\frac{J_2 t_a}{MU_{ab}} (2 S_i^x) \left(\frac{M}{2} + S_{i+1}^z \right) - \frac{J_2 t_a}{MU_{ab}} (2 S_{i-1}^x) \left(\frac{M}{2} + 1 + S_i^z \right) \\
&= -\frac{z J_2 t_a}{MU_{ab}} ((M+1) S_i^x + 2 S_i^x S_{i+1}^z) \\
(d) &= -J_2 t_b P \left[n_{b,i-1} \left(a_i \frac{Q}{QHQP-PHP} b_i^+ + b_i \frac{Q}{QHQP-PHP} a_i^+ \right) \right. \\
&\quad \left. + (a_{i+1}^+ b_{i+1} + b_{i+1}^+ a_{i+1}) b_i \frac{Q}{QHQP-PHP} b_i^+ \right] P \\
&= -\frac{J_2 t_b}{MU_{ab}} (2 S_i^x) \left(\frac{M}{2} - S_{i-1}^z \right) - \frac{J_2 t_b}{MU_{ab}} (2 S_{i+1}^x) \left(\frac{M}{2} + 1 - S_i^z \right) \\
&= -\frac{z J_2 t_b}{MU_{ab}} ((M+1) S_i^x - 2 S_i^x S_{i+1}^z)
\end{aligned}$$

The effective Hamiltonian, scaled by $M(= 2S)$:

$$H_{\text{eff}} = \mu \sum_i (S_i^z)^2 - z(2S+1) \sum_i \frac{(t_a^2 - t_b^2)}{U_{ab}} S_i^z - z(2S+1) \sum_i \frac{J_2(t_a + t_b)}{U_{ab}} S_i^x - \frac{2(t_a^2 + t_b^2 - J_2^2)}{U_{ab}} \sum_i S_i^z S_{i+1}^z \\ - \frac{4t_a t_b}{U_{ab}} \sum_i (S_i^x S_{i+1}^x + S_i^y S_{i+1}^y) - \frac{4J_2 t_a}{U_{ab}} \sum_i S_i^x S_{i+1}^z + \frac{4J_2 t_b}{U_{ab}} \sum_i S_i^z S_{i+1}^x$$

-
- [1] I. Bloch, J. Dalibard, and S. Nascimbène, *Nat. Phys.* **8**, 267 (2012).
- [2] M. Lewenstein, A. Sanpera, V. Ahufinger, B. Damski, A. Sen(De), and U. Sen, *Advances in Physics* **56**, 243 (2007).
- [3] M. Greiner, O. Mandel, T. Esslinger, T. W. Hänsch, and I. Bloch, *Nature* **415**, 39 (2002).
- [4] S. Sachdev, *Quantum Phase Transitions* (Cambridge University Press, 2000).
- [5] I. Bloch, J. Dalibard, and W. Zwerger, *Rev. Mod. Phys.* **80**, 885 (2008).
- [6] T. Esslinger, *Annu. Rev. Condens. Matter Phys.* **1**, 129 (2010).
- [7] C. Weitenberg, M. Endres, J. F. Sherson, M. Cheneau, P. Schauß, T. Fukuhara, I. Bloch, and S. Kuhr, *Nature* **471**, 319 (2011).
- [8] D. Jaksch, C. Bruder, J. I. Cirac, C. W. Gardiner, and P. Zoller, *Phys. Rev. Lett.* **81**, 3108 (1998).
- [9] O. Morsch and M. Oberthaler, *Rev. Mod. Phys.* **78**, 179 (2006).
- [10] D. C. McKay and B. DeMarco, *Rep. Prog. Phys.* **74**, 054401 (2011).
- [11] B. Capogrosso-Sansone, Ş. G. Söyler, N. V. Prokof'ev, and B. V. Svistunov, *Phys. Rev. A* **81**, 053622 (2010).
- [12] R. Jördens, L. Tarruell, D. Greif, T. Uehlinger, N. Strohmaier, H. Moritz, T. Esslinger, L. D. Leo, C. Kollath, A. Georges, V. Scarola, L. Pollet, E. Burovski, E. Kozik, and M. Troyer, *Phys. Rev. Lett.* **104**, 180401 (2010).
- [13] S. Fölling, S. Trotzky, P. Cheinet, M. Feld, R. Saers, A. Widera, T. Müller, and I. Bloch, *Nature* **448**, 1029 (2007).
- [14] T.-L. Ho and Q. Zhou, *Phys. Rev. Lett.* **99**, 120404 (2007).
- [15] P. Medley, D. M. Weld, H. Miyake, D. E. Pritchard, and W. Ketterle, *Phys. Rev. Lett.* **106**, 195301 (2011).
- [16] P. Rabl, A. J. Daley, P. O. Fedichev, J. I. Cirac, and P. Zoller, *Phys. Rev. Lett.* **91**, 110403 (2003).
- [17] S. Trebst, U. Schollwöck, M. Troyer, and P. Zoller, *Phys. Rev. Lett.* **96**, 250402 (2006).
- [18] A. Kantian, A. J. Daley, and P. Zoller, *Phys. Rev. Lett.* **104**, 240406 (2010).
- [19] M. Lubasch, V. Murg, U. Schneider, J. I. Cirac, and M.-C. Bañuls, *Phys. Rev. Lett.* **107**, 165301 (2011).
- [20] A. S. Sørensen, E. Altman, M. Gullans, J. V. Porto, M. D. Lukin, and E. Demler, *Phys. Rev. A* **81**, 061603 (2010).
- [21] S. Gammelmark and A. Eckardt, *New J. Phys.* **15**, 033028 (2013).
- [22] J. Dalibard, F. Gerbier, G. Juzeliūnas, and P. Öhberg, *Rev. Mod. Phys.* **83**, 1523 (2011).
- [23] N. Goldman, G. Juzeliūnas, P. Öhberg, and I. B. Spielman, *Rep. Prog. Phys.* **77**, 126401 (2014).
- [24] G.-B. Jo, Y.-R. Lee, J.-H. Choi, C. A. Christensen, T. H. Kim, J. H. Thywissen, D. E. Pritchard, and W. Ketterle, *Science* **325**, 1521 (2009).
- [25] J. Struck, C. Ölschläger, R. Le Targat, P. Soltan-Panahi, A. Eckardt, M. Lewenstein, P. Windpassinger, and K. Sengstock, *Science* **333**, 996 (2011).
- [26] A. Eckardt, C. Weiss, and M. Holthaus, *Phys. Rev. Lett.* **95**, 260404 (2005).
- [27] S. Sachdev, K. Sengupta, and S. M. Girvin, *Phys. Rev. B* **66**, 075128 (2002).
- [28] J. Simon, W. S. Bakr, R. Ma, M. E. Tai, P. M. Preiss, and M. Greiner, *Nature* **472**, 307 (2011).
- [29] S. Pielawa, T. Kitagawa, E. Berg, and S. Sachdev, *Phys. Rev. B* **83**, 205135 (2011).
- [30] M. P. A. Fisher, P. B. Weichman, G. Grinstein, and D. S. Fisher, *Phys. Rev. B* **40**, 546 (1989).
- [31] M. Lewenstein, A. Sanpera, and V. Ahufinger, *Ultracold Atoms in Optical Lattices* (Oxford University Press, 2012).
- [32] A. Aspuru-Guzik and P. Walther, *Nat. Phys.* **8**, 285 (2012).
- [33] R. Blatt and C. F. Roos, *Nat. Phys.* **8**, 277 (2012).
- [34] J. I. Cirac and P. Zoller, *Nat. Phys.* **8**, 264 (2012).
- [35] P. Hauke, F. M. Cucchietti, L. Tagliacozzo, I. Deutsch, and M. Lewenstein, *Rep. Prog. Phys.* **75**, 082401 (2012).
- [36] A. A. Houck, H. E. Türeci, and J. Koch, *Nat. Phys.* **8**, 292 (2012).
- [37] C. Gross and I. Bloch, *Science* **357**, 995 (2017).
- [38] A. B. Kuklov and B. V. Svistunov, *Phys. Rev. Lett.* **90**, 100401 (2003).
- [39] E. Altman, W. Hofstetter, E. Demler, and M. D. Lukin, *New J. Phys.* **5**, 113 (2003).
- [40] J. J. García-Ripoll, M. A. Martin-Delgado, and J. I. Cirac, *Phys. Rev. Lett.* **93**, 250405 (2004).
- [41] E. G. D. Torre, E. Berg, and E. Altman, *Phys. Rev. Lett.* **97**, 260401 (2006).
- [42] E. Berg, E. G. D. Torre, T. Giamarchi, and E. Altman, *Phys. Rev. B* **77**, 245119 (2008).
- [43] L. Amico, G. Mazzarella, S. Pasini, and F. S. Cataliotti, *New J. Phys.* **12**, 013002 (2010).
- [44] M. Dalmonte, M. D. Dio, L. Barbiero, and F. Ortolani, *Phys. Rev. B* **83**, 155110 (2011).
- [45] D. Rossini and R. Fazio, *New J. Phys.* **14**, 065012 (2012).
- [46] C. Trefzger, C. Menotti, and M. Lewenstein, *Phys. Rev. A* **78**, 043604 (2008).
- [47] X.-F. Zhou, Z.-X. Chen, Z.-W. Zhou, Y.-S. Zhang, and G.-C. Guo, *Phys. Rev. A* **81**, 021602 (2010).
- [48] J. Jin, D. Rossini, R. Fazio, M. Leib, and M. J. Hartmann, *Phys. Rev. Lett.* **110**, 163605 (2013).

- [49] T. Mishra, R. V. Pai, S. Ramanan, M. S. Luthra, and B. P. Das, *Phys. Rev. A* **80**, 043614 (2009).
- [50] M. Kumar, S. Sarkar, and S. Ramasesha, *Int. J. Mod. Phys. B* **25**, 159 (2011).
- [51] R. Bai, D. Gaur, H. Sable, S. Bandyopadhyay, K. Suthar, and D. Angom, *Physical Review A* **102**, 10.1103/physreva.102.043309 (2020).
- [52] D. M. Stamper-Kurn, M. R. Andrews, A. P. Chikkatur, S. Inouye, H.-J. Miesner, J. Stenger, and W. Ketterle, *Phys. Rev. Lett.* **80**, 2027 (1998).
- [53] D. M. Stamper-Kurn and M. Ueda, *Rev. Mod. Phys.* **85**, 1191 (2013).
- [54] K. V. Krutitsky and R. Graham, *Phys. Rev. A* **70**, 063610 (2004).
- [55] T. Kimura, S. Tsuchiya, and S. Kurihara, *Phys. Rev. Lett.* **94**, 110403 (2005).
- [56] Q. Zhou, J. V. Porto, and S. D. Sarma, *Phys. Rev. B* **83**, 195106 (2011).
- [57] J. Pietraszewicz, T. Sowiński, M. Brewczyk, J. Zakrzewski, M. Lewenstein, and M. Gajda, *Phys. Rev. A* **85**, 053638 (2012).
- [58] X. Li, Z. Zhang, and W. V. Liu, *Phys. Rev. Lett.* **108**, 175302 (2012).
- [59] T. Sowiński, M. Łącki, O. Dutta, J. Pietraszewicz, P. Sierant, M. Gajda, J. Zakrzewski, and M. Lewenstein, *Phys. Rev. Lett.* **111**, 215302 (2013).
- [60] L.-M. Duan, E. Demler, and M. D. Lukin, *Phys. Rev. Lett.* **91**, 090402 (2003).
- [61] D. Giuliano, D. Rossini, P. Sodano, and A. Trombettoni, *Phys. Rev. B* **87**, 035104 (2013).
- [62] S. Powell, *Phys. Rev. A* **79**, 053614 (2009).
- [63] A. Hubener, M. Snoek, and W. Hofstetter, *Phys. Rev. B* **80**, 245109 (2009).
- [64] Y. Nakano, T. Ishima, N. Kobayashi, T. Yamamoto, I. Ichinose, and T. Matsui, *Phys. Rev. A* **85**, 023617 (2012).
- [65] G. Thalhammer, G. Barontini, L. D. Sarlo, J. Catani, F. Minardi, and M. Inguscio, *Phys. Rev. Lett.* **100**, 210402 (2008).
- [66] J. Klinder, H. Keßler, M. R. Bakhtiari, M. Thorwart, and A. Hemmerich, *Phys. Rev. Lett.* **115**, 230403 (2015).
- [67] R. Landig, L. Hruby, N. Dogra, M. Landini, R. Mottl, T. Donner, and T. Esslinger, *Nature* **532**, 476 (2016).
- [68] C. Kollath, A. Sheikhan, S. Wolff, and F. Brennecke, *Phys. Rev. Lett.* **116**, 060401 (2016).
- [69] F. Mivehvar, H. Ritsch, and F. Piazza, *Phys. Rev. Lett.* **118**, 073602 (2017).
- [70] A. Sheikhan and C. Kollath, *Phys. Rev. A* **99**, 053611 (2019).
- [71] F. Schlawin, A. Cavalleri, and D. Jaksch, *Phys. Rev. Lett.* **122**, 133602 (2019).
- [72] F. Schlawin and D. Jaksch, *Phys. Rev. Lett.* **123**, 133601 (2019).
- [73] J. B. Curtis, Z. M. Raines, A. A. Allocca, M. Hafezi, and V. M. Galitski, *Phys. Rev. Lett.* **122**, 167002 (2019).
- [74] G. Mazza and A. Georges, *Phys. Rev. Lett.* **122**, 017401 (2019).
- [75] E. Colella, S. Ostermann, W. Niedenzu, F. Mivehvar, and H. Ritsch, *New J. Phys.* **21**, 043019 (2019).
- [76] S. Uchino, M. Ueda, and J.-P. Brantut, *Phys. Rev. A* **98**, 063619 (2018).
- [77] C. J. Pethick and H. Smith, *Bose–Einstein Condensation in Dilute Gases* (Cambridge University Press, 2001).
- [78] M. R. Matthews, D. S. Hall, D. S. Jin, J. R. Ensher, C. E. Wieman, E. A. Cornell, F. Dalfovo, C. Minniti, and S. Stringari, *Phys. Rev. Lett.* **81**, 243 (1998).
- [79] T. Zibold, E. Nicklas, C. Gross, and M. K. Oberthaler, *Phys. Rev. Lett.* **105**, 204101 (2010).
- [80] E. Nicklas, H. Strobel, T. Zibold, C. Gross, B. A. Malomed, P. G. Kevrekidis, and M. K. Oberthaler, *Phys. Rev. Lett.* **107**, 193001 (2011).
- [81] P. B. Blakie, R. J. Ballagh, and C. W. Gardiner, *J. Opt. B Quantum Semiclassical Opt.* **1**, 378 (1999).
- [82] C. P. Search and P. R. Berman, *Phys. Rev. A* **63**, 043612 (2001).
- [83] P. Tommasini, E. J. V. de Passos, A. F. R. de Toledo Piza, M. S. Hussein, and E. Timmermans, *Phys. Rev. A* **67**, 023606 (2003).
- [84] C. Lee, W. Hai, L. Shi, and K. Gao, *Phys. Rev. A* **69**, 033611 (2004).
- [85] I. M. Merhasin, B. A. Malomed, and R. Driben, *J. Phys. B: At. Mol. Opt. Phys.* **38**, 877 (2005).
- [86] M. Abad and A. Recati, *Eur. Phys. J. D* **67**, (2013).
- [87] S. Butera, P. Öhberg, and I. Carusotto, *Phys. Rev. A* **96**, 013611 (2017).
- [88] Z. Chen and B. A. Malomed, *Phys. Rev. E* **95**, 032217 (2017).
- [89] G. Shchedrin, D. Jaschke, and L. D. Carr, *Phys. Rev. A* **97**, 043601 (2018).
- [90] U. Bornheimer, I. Vasić, and W. Hofstetter, *Phys. Rev. A* **96**, 063623 (2017).
- [91] I. Morera, A. Polls, and B. Juliá-Díaz, *Sci. Rep.* **9**, 9424 (2019).
- [92] B. V. Chirikov, *Phys. Rep.* **52**, 263 (1979).
- [93] A. Buchleitner, D. Delande, and J. Zakrzewski, *Phys. Rep.* **368**, 409 (2002).
- [94] M. Hiller, H. Venzl, T. Zech, B. Oleś, F. Mintert, and A. Buchleitner, *J. Phys. B: At. Mol. Opt. Phys.* **45**, 095301 (2012).
- [95] J. Schachenmayer, D. M. Weld, H. Miyake, G. A. Siviloglou, W. Ketterle, and A. J. Daley, *Phys. Rev. A* **92**, 041602 (2015).
- [96] Y. Kuno, I. Ichinose, and Y. Takahashi, *Sci. Rep.* **8**, 10699 (2018).
- [97] D. Jaksch and P. Zoller, *New J. Phys.* **5**, 56 (2003).
- [98] S. Al-Assam, S. R. Clark, C. J. Foot, and D. Jaksch, *Phys. Rev. B* **84**, 205108 (2011).
- [99] F. Mezzacapo, N. Schuch, M. Boninsegni, and J. I. Cirac, *New J. Phys.* **11**, 083026 (2009).
- [100] S. de Léséleuc, V. Lienhard, P. Scholl, D. Barredo, S. Weber, N. Lang, H. P. Büchler, T. Lahaye, and A. Browaeys, *Science* **365**, 775 (2019).
- [101] M. Aidelsburger, M. Atala, M. Lohse, J. T. Barreiro, B. Paredes, and I. Bloch, *Physical Review Letters* **111**, 10.1103/physrevlett.111.185301 (2013).
- [102] E. Urban, T. A. Johnson, T. Henage, L. Isenhower, D. Yavuz, T. Walker, and M. Saffman, *Nat. Phys.* **5**, 110 (2009).
- [103] M. A. Cazalilla, *Phys. Rev. A* **67**, 053606 (2003).